Supplement of Earth Syst. Sci. Data, 18, 8037–8105, 2026
https://doi.org/10.5194/essd-18-8037-2026-supplement
© Author(s) 2026. CC BY 4.0 License.



Open Access Earth System Science Data

Supplement of

State of Wildfires 2025–2026

Chantelle A. Burton et al.

Correspondence to: Chantelle A. Burton (chantelle.burton@metoffice.gov.uk), Francesca Di Giuseppe (francesca.digiuseppe@ecmwf.int), Matthew W. Jones (matthew.w.jones@uea.ac.uk), and Douglas I. Kelley (doukel@ceh.ac.uk)

The copyright of individual parts of the supplement might differ from the article licence.

S1. Methods and Evaluation

S1.1. Hydroclimatic Drivers

Table S1: Input features used to derive hydroclimatic anomalies and the driver attribution in PoF. In some cases, native data was regridded from higher resolution to coarse resolution for use in the model.

Variable	Category	Source	Reference
High Vegetation Cover	Fuel	CONFESS	Boussetta et al., 2021
Low Vegetation Cover	Fuel	CONFESS	Boussetta et al., 2021
Type of High Vegetation	Fuel	CONFESS	Boussetta et al., 2021
Type of Low Vegetation	Fuel	CONFESS	Boussetta et al., 2021
High Vegetation LAI	Fuel	CGLS	Copernicus Global Land Service, 2026
Low Vegetation LAI	Fuel	CGLS	Copernicus Global Land Service, 2026
Dead Foliage Load	Fuel	Sparky-Fuel	McNorton & Di Giuseppe, 2024
Dead Wood Load	Fuel	Sparky-Fuel	McNorton & Di Giuseppe, 2024
Live Leaf Load	Fuel	Sparky-Fuel	McNorton & Di Giuseppe, 2024
Live Wood Load	Fuel	Sparky-Fuel	McNorton & Di Giuseppe, 2024
Dead Foliage Moisture	Fuel	Sparky-Fuel	McNorton & Di Giuseppe, 2024
Dead Wood Moisture	Fuel	Sparky-Fuel	McNorton & Di Giuseppe, 2024
Live Fuel Moisture	Fuel	Sparky-Fuel	McNorton & Di Giuseppe, 2024
2m Temperature	Weather	ERA5 Land	Muñoz-Sabater et al., 2021
Wind Speed	Weather	ERA5 Land	Muñoz-Sabater et al., 2021
Relative Humidity	Weather	ERA5 Land	Muñoz-Sabater et al., 2021
Total Precipitation	Weather	ERA5 Land	Muñoz-Sabater et al., 2021
Orography		ECLand	Boussetta et al., 2021
Population Density	Ign-Supp	GPW v4 – SEDAC	CIESIN, 2017
Nightlights	Ign-Supp	Harmonized Global Nighttime Light	Li et al., 2020
Gross Domestic Product	Ign-Supp	Our World in Data	Kummu et al., 2025
Human Development Index	Ign-Supp	UNDP Human Development Report	Liu et al., 2024
Road Density	Ign-Supp	Global Roads Inventory Dataset	Meijer et al., 2018
Terrestrial Biome Protection	Ign-Supp	EPI - Yale	Block et al., 2024
Government Effectiveness	Ign-Supp	Our World in Data	World Bank, 2025
Urban Cover	Ign-Supp	GHSL	Pesaresi & Politis, 2025
Lightning	Ign-Supp	IFS	Lopez, 2016

S1.2. Influence of Climate Change on Focal Events

S1.2.1. Attribution of Present Day Focal Events - FWI

For the FWI WWA multi-model analysis, we assess the performance of each climate model dataset regionally using a qualitative comparison of the seasonal cycle and spatial pattern for a 1990-2019 climatology, and the parameters of the fitted statistical models. Each of these three criteria were rated as 'good', 'reasonable' or 'bad' – with a model rated as 'good' if 'good' in all three properties, 'bad' if 'bad' in any property, and 'reasonable' otherwise. Whilst we would ideally only use 'good' models, the low number of these meant that 'reasonable' models were also considered. We show the full model evaluation in the tables below.

Table S2: Model evaluation for FWI95 – Midwest Canadian Forest Shield. Evaluation results of the climate models considered for attribution analysis of FWI95 in the Midwest Canadian Forest Shield region. For each model, the best estimates of the Scale and Shape parameters of the GEV are shown, along with 95% confidence intervals. If the best estimate of these parameters falls within the 95% CI for the reanalysis, the model was evaluated as good; else if the 95% CIs of the model and reanalysis overlapped it was rated as reasonable; and otherwise was rated as a bad representation of the extreme FWI95 distribution. Furthermore evaluation of the seasonal cycle and spatial pattern are shown, which were evaluated by visual comparison of the seasonal and geospatial climatology to reanalysis patterns – comparison figures available on zenodo. The lowest realisation member of each model with all "good" ratings was included in the final analysis, if there was no realisation meeting that criteria, the lowest overall "reasonable" model was included.

				Scale parameter Obs Min: 0.151 Obs Max: 0.303			**Shape parameter Obs Min: -0.553 Obs Max: -0.0322**						
Model	**Member**	**Seasonal cycle**	**Spatial pattern**	Best estimate	Lower bound	Upper bound	Best estimate	Lower bound	Upper bound	**Sigma**	**Shape**	**Rating**	**Model Inclusion**
AWI-ESM-1-REcoM	r1i1p1f1	bad	good	0.419	0.331	0.476	-0.131	-0.578	0.277	bad	good	bad	**N**
CanESM5	r1i1p2f1	good	good	0.174	0.129	0.201	0.060	-0.200	0.427	good	reasonable	reasonable	**N**
CanESM5	r8i1p1f1	good	good	0.182	0.138	0.213	-0.068	-0.332	0.217	good	good	good	**Y**
CNRM-CM6-1-HR	r1i1p1f2	reasonable	good	0.206	0.163	0.238	-0.340	-0.645	-0.121	good	good	reasonable	**N**
CNRM-CM6-1	r1i1p1f2	reasonable	good	0.201	0.160	0.230	-0.219	-0.475	0.043	good	good	reasonable	**N**
CNRM-ESM2-1	r1i1p1f2	reasonable	good	0.164	0.129	0.195	-0.545	-0.764	-0.389	good	good	reasonable	**Y**
GFDL-CM4	r1i1p1f1	good	good	0.164	0.126	0.190	0.281	-0.186	0.575	good	reasonable	reasonable	**Y**
INM-CM4-8	r1i1p1f1	bad	reasonable	0.315	0.261	0.352	0.037	-0.179	0.248	reasonable	reasonable	bad	**N**
INM-CM5-0	r1i1p1f1	bad	reasonable	0.307	0.214	0.349	0.001	-0.156	0.277	reasonable	reasonable	bad	**N**
MIROC6	r1i1p1f1	good	reasonable	0.116	0.089	0.136	-0.136	-0.426	0.068	bad	good	bad	**N**
MIROC6	r2i1p1f1	good	reasonable	0.138	0.112	0.157	-0.155	-0.428	0.068	reasonable	good	reasonable	**Y**
MIROC6	r3i1p1f1	good	reasonable	0.157	0.116	0.185	-0.303	-0.716	-0.166	good	good	reasonable	**N**
MPI-ESM1-2-LR	r10i1p1f1	reasonable	reasonable	0.403	0.327	0.461	0.184	-0.064	0.423	bad	reasonable	bad	**N**
MPI-ESM1-2-LR	r11i1p1f1	reasonable	reasonable	0.305	0.234	0.361	-0.158	-0.382	0.018	reasonable	good	reasonable	**N**
MPI-ESM1-2-LR	r12i1p1f1	reasonable	reasonable	0.275	0.216	0.319	0.321	0.091	0.550	good	reasonable	reasonable	**N**
MPI-ESM1-2-LR	r13i1p1f1	good	bad	0.318	0.241	0.358	0.002	-0.310	0.376	reasonable	reasonable	bad	**N**
MPI-ESM1-2-LR	r14i1p1f1	reasonable	bad	0.397	0.293	0.463	0.042	-0.113	0.280	reasonable	reasonable	bad	**N**
MPI-ESM1-2-LR	r15i1p1f1	good	bad	0.358	0.291	0.406	0.033	-0.182	0.196	reasonable	reasonable	bad	**N**
MPI-ESM1-2-LR	r16i1p1f1	good	bad	0.272	0.214	0.312	0.233	0.028	0.492	good	reasonable	bad	**N**
MPI-ESM1-2-LR	r17i1p1f1	reasonable	bad	0.344	0.268	0.395	0.113	-0.098	0.357	reasonable	reasonable	bad	**N**
MPI-ESM1-2-LR	r18i1p1f1	reasonable	bad	0.302	0.214	0.352	-0.272	-0.493	0.150	good	good	bad	**N**
MPI-ESM1-2-LR	r19i1p1f1	good	bad	0.324	0.244	0.378	-0.020	-0.216	0.211	reasonable	reasonable	bad	**N**

MPI-ESM1-2-LR	r1i1p1f1	good	reasonable	0.334	0.263	0.389	-0.065	-0.272	0.104	reasonable	good	reasonable	N
MPI-ESM1-2-LR	r20i1p1f1	good	reasonable	0.290	0.234	0.333	0.081	-0.132	0.286	good	reasonable	reasonable	N
MPI-ESM1-2-LR	r21i1p1f1	good	bad	0.404	0.319	0.460	-0.152	-0.372	0.025	bad	good	bad	N
MPI-ESM1-2-LR	r22i1p1f1	good	reasonable	0.345	0.266	0.396	0.096	-0.225	0.388	reasonable	reasonable	reasonable	N
MPI-ESM1-2-LR	r23i1p1f1	good	bad	0.314	0.238	0.360	0.209	-0.143	0.660	reasonable	reasonable	bad	N
MPI-ESM1-2-LR	r24i1p1f1	good	bad	0.340	0.268	0.384	0.204	-0.044	0.502	reasonable	reasonable	bad	N
MPI-ESM1-2-LR	r25i1p1f1	reasonable	bad	0.331	0.265	0.378	-0.055	-0.570	0.170	reasonable	good	bad	N
MPI-ESM1-2-LR	r26i1p1f1	good	bad	0.343	0.271	0.409	0.334	-0.022	0.573	reasonable	reasonable	bad	N
MPI-ESM1-2-LR	r27i1p1f1	reasonable	bad	0.336	0.269	0.378	0.038	-0.357	0.214	reasonable	reasonable	bad	N
MPI-ESM1-2-LR	r28i1p1f1	good	reasonable	0.342	0.274	0.388	0.028	-0.198	0.240	reasonable	reasonable	reasonable	N
MPI-ESM1-2-LR	r29i1p1f1	good	bad	0.287	0.227	0.321	0.167	-0.023	0.438	good	reasonable	bad	N
MPI-ESM1-2-LR	r2i1p1f1	good	bad	0.222	0.175	0.268	0.271	-0.072	0.503	good	reasonable	bad	N
MPI-ESM1-2-LR	r30i1p1f1	good	bad	0.289	0.215	0.336	0.003	-0.171	0.189	good	reasonable	bad	N
MPI-ESM1-2-LR	r31i1p1f1	good	reasonable	0.266	0.207	0.305	0.161	-0.026	0.384	good	reasonable	reasonable	N
MPI-ESM1-2-LR	r32i1p1f1	good	bad	0.344	0.242	0.404	-0.063	-0.392	0.112	reasonable	good	bad	N
MPI-ESM1-2-LR	r33i1p1f1	good	bad	0.275	0.210	0.321	0.308	0.085	0.572	good	reasonable	bad	N
MPI-ESM1-2-LR	r34i1p1f1	reasonable	bad	0.343	0.270	0.398	-0.360	-0.621	-0.200	reasonable	good	bad	N
MPI-ESM1-2-LR	r35i1p1f1	good	bad	0.378	0.291	0.439	0.050	-0.153	0.257	reasonable	reasonable	bad	N
MPI-ESM1-2-LR	r36i1p1f1	reasonable	reasonable	0.374	0.286	0.409	0.083	-0.292	0.742	reasonable	reasonable	reasonable	N
MPI-ESM1-2-LR	r37i1p1f1	reasonable	reasonable	0.373	0.309	0.414	-0.058	-0.512	0.125	bad	good	bad	N
MPI-ESM1-2-LR	r38i1p1f1	good	bad	0.246	0.196	0.282	0.214	-0.012	0.444	good	reasonable	bad	N
MPI-ESM1-2-LR	r39i1p1f1	reasonable	bad	0.279	0.226	0.317	0.013	-0.192	0.245	good	reasonable	bad	N
MPI-ESM1-2-LR	r3i1p1f1	reasonable	reasonable	0.327	0.260	0.362	-0.023	-0.223	0.267	reasonable	reasonable	reasonable	N
MPI-ESM1-2-LR	r40i1p1f1	good	good	0.247	0.193	0.285	-0.120	-0.302	0.041	good	good	good	Y
MPI-ESM1-2-LR	r41i1p1f1	reasonable	reasonable	0.309	0.228	0.353	0.176	-0.049	0.463	reasonable	reasonable	reasonable	N
MPI-ESM1-2-LR	r42i1p1f1	reasonable	bad	0.287	0.219	0.347	0.320	-0.126	0.663	good	reasonable	bad	N
MPI-ESM1-2-LR	r43i1p1f1	reasonable	reasonable	0.306	0.226	0.351	0.069	-0.269	0.459	reasonable	reasonable	reasonable	N
MPI-ESM1-2-LR	r44i1p1f1	reasonable	good	0.332	0.264	0.382	0.122	-0.165	0.363	reasonable	reasonable	reasonable	N
MPI-ESM1-2-LR	r45i1p1f1	good	bad	0.332	0.249	0.377	0.170	-0.069	0.454	reasonable	reasonable	bad	N
MPI-ESM1-2-LR	r46i1p1f1	good	bad	0.373	0.280	0.427	0.155	-0.017	0.359	reasonable	reasonable	bad	N
MPI-ESM1-2-LR	r47i1p1f1	reasonable	bad	0.318	0.246	0.367	-0.039	-0.331	0.102	reasonable	good	bad	N
MPI-ESM1-2-LR	r48i1p1f1	reasonable	reasonable	0.322	0.256	0.364	0.199	-0.056	0.439	reasonable	reasonable	reasonable	N
MPI-ESM1-2-LR	r49i1p1f1	reasonable	bad	0.300	0.244	0.340	0.162	-0.150	0.394	good	reasonable	bad	N
MPI-ESM1-2-LR	r4i1p1f1	reasonable	bad	0.334	0.233	0.380	0.189	-0.052	0.741	reasonable	reasonable	bad	N
MPI-ESM1-2-LR	r50i1p1f1	good	reasonable	0.256	0.195	0.297	0.291	0.062	0.529	good	reasonable	reasonable	N
MPI-ESM1-2-LR	r5i1p1f1	good	bad	0.274	0.153	0.316	0.256	0.045	1.145	good	reasonable	bad	N
MPI-ESM1-2-LR	r6i1p1f1	reasonable	good	0.322	0.259	0.362	0.164	-0.047	0.418	reasonable	reasonable	reasonable	N
MPI-ESM1-2-LR	r7i1p1f1	good	reasonable	0.250	0.192	0.305	0.206	-0.325	0.506	good	reasonable	reasonable	N
MPI-ESM1-2-LR	r8i1p1f1	reasonable	good	0.369	0.272	0.426	0.111	-0.145	0.356	reasonable	reasonable	reasonable	N
MPI-ESM1-2-LR	r9i1p1f1	reasonable	reasonable	0.34261 14982	0.247 52963 08	0.396 98478 17	0.23926 32176	0.023 92924 717	0.5608 02780 9	reasonable	reasonable	reasonable	N

MRI-ESM2-0	r1i1p1f1	good	good	0.18576 49706	0.1411 74591 5	0.214 54001 45	0.21685 48831	-0.011 87444 286	0.5364 71386 9	good	reasonable	reasonable	**Y**
CNRM-CM6-1-HR	r1i1p1f2	reasonable, peak increases not decreases	good	0.18221 75184	0.140 66093 06	0.213 92866 32	-0.14879 24774	-0.479 53327 81	0.1115 79290 5	good	good	reasonable	**Y**
CNRM-CM6-1	r1i1p1f2	reasonable, peak increases not decreases	good	0.165	0.129	0.193	-0.495	-0.831	-0.269	good	good	reasonable	**Y**
EC-Earth3P-HR	r1i1p1f1	good	good	0.181	0.168	0.194	-0.202	-0.508	-0.179	good	good	good	**Y**
EC-Earth3P-HR	r2i1p1f1	good	good	0.183	0.141	0.212	-0.066	-0.340	0.294	good	good	good	**N**
EC-Earth3P-HR	r3i1p1f1	good	good	0.205	0.165	0.232	0.009	-0.630	0.169	good	reasonable	reasonable	**N**
EC-Earth3P	r1i1p1f1	good	good	0.186	0.175	0.195	-0.382	-0.457	-0.310	good	good	good	**Y**
EC-Earth3P	r2i1p1f1	good	good	0.198	0.161	0.223	-0.097	-0.281	0.072	good	good	good	**N**
EC-Earth3P	r3i1p1f1	good	good	0.190	0.140	0.217	0.020	-0.153	0.230	good	reasonable	reasonable	**N**
HadGEM3-GC31-HM	r1i1p1f1	reasonable, peak increases not decreases	good	0.205	0.170	0.231	-0.106	-0.296	0.074	good	good	reasonable	**Y**
HadGEM3-GC31-HM	r1i2p1f1	reasonable, peak increases not decreases	good	0.174	0.142	0.201	-0.121	-0.563	0.110	good	good	reasonable	**N**
HadGEM3-GC31-HM	r1i3p1f1	reasonable, peak increases not decreases	good	0.202	0.162	0.237	-0.075	-0.349	0.130	good	good	reasonable	**N**
HadGEM3-GC31-LM	r1i1p1f1	reasonable, summer a little flat	good	0.179	0.138	0.206	-0.046	-0.255	0.154	good	good	reasonable	**Y**
HadGEM3-GC31-MM	r1i1p1f1	reasonable, summer a little flat	good	0.15104 0039	0.108 21685 7	0.175 73427 71	0.09890 227433	-0.220 17941 02	0.4591 78578 6	reasonable	reasonable	reasonable	**Y**
HadGEM3-GC31-MM	r1i2p1f1	reasonable, summer a little flat	good	0.21090 31524	0.174 69750 48	0.238 37606 21	-0.35044 69311	-0.597 66480 15	-0.112 82782 83	good	good	reasonable	**N**
HadGEM3-GC31-MM	r1i3p1f1	reasonable, summer a little flat	good	0.18493 22386	0.143 14204 47	0.215 06401 46	0.18903 42515	-0.023 60962 646	0.4358 12871 9	good	reasonable	reasonable	**N**

Table S3: Model evaluation for FWI95 – Northwest Iberia. Evaluation results of the climate models considered for attribution analysis of FWI95 in the Northwest Iberia region. For each model, the best estimates of the Scale and Shape parameters of the GEV are shown, along with 95% confidence intervals. If the best estimate of these parameters falls within the 95% CI for the reanalysis, the model was evaluated as good; else if the 95% CIs of the model and reanalysis overlapped it was rated as reasonable; and otherwise was rated as a bad representation of the extreme FWI95 distribution. Furthermore evaluation of the seasonal cycle and spatial pattern are shown, which were evaluated by visual comparison of the seasonal and geospatial climatology to reanalysis patterns – comparison figures available on zenodo. The lowest realisation member of each model with all "good" ratings was included in the final analysis, if there was no realisation meeting that criteria, the lowest overall "reasonable" model was included.

Model	Member	Seasonal cycle	Spatial pattern	Sigma parameter Obs Min: 0.0734 Obs Max: 0.142			Shape parameter Obs Min: -0.890 Obs Max: -0.269			Sigma	Shape	Rating	Model Inclusion
				Best estimate	Lower bound	Upper bound	Best estimate	Lower bound	Upper bound				
AWI-ESM-1-REcoM	r1i1p1f1	good	reasonable	0.124	0.090	0.151	-0.307	-0.626	-0.069	reasonable	good	reasonable	**Y**
CanESM5	r1i1p2f1	good	bad	0.156	0.120	0.186	-0.565	-0.765	-0.384	bad	good	bad	**N**
CanESM5	r8i1p1f1	good	bad	0.111	0.081	0.135	-0.327	-0.654	-0.054	reasonable	good	bad	**N**
CNRM-CM6-1-HR	r1i1p1f2	good	good	0.204	0.155	0.243	-0.545	-0.781	-0.324	bad	good	bad	**N**
CNRM-CM6-1	r1i1p1f2	good	reasonable	0.154	0.119	0.176	-0.534	-0.732	-0.339	bad	good	bad	**N**
CNRM-ESM2-1	r1i1p1f2	good	reasonable	0.145	0.110	0.175	-0.492	-0.746	-0.387	bad	good	bad	**Y**
GFDL-CM4	r1i1p1f1	good	good	0.274	0.202	0.341	-0.634	-0.872	-0.427	bad	bad	bad	**N**
INM-CM4-8	r1i1p1f1	good	reasonable	0.071	0.057	0.082	-0.408	-0.570	-0.273	good	good	reasonable	**Y**
INM-CM5-0	r1i1p1f1	good	reasonable	0.089	0.058	0.109	-0.356	-0.625	-0.039	good	good	reasonable	**Y**
MIROC6	r1i1p1f1	good	reasonable	0.102	0.082	0.120	-0.445	-0.697	-0.335	good	good	reasonable	**Y**
MIROC6	r2i1p1f1	good	reasonable	0.117	0.085	0.136	-0.232	-0.443	0.059	reasonable	good	reasonable	**N**
MIROC6	r3i1p1f1	good	reasonable	0.137	0.081	0.176	-0.344	-0.642	-0.041	reasonable	good	reasonable	**N**
MPI-ESM1-2-LR	r10i1p1f1	good	reasonable	0.149	0.124	0.169	-0.083	-0.383	0.108	bad	good	bad	**N**
MPI-ESM1-2-LR	r11i1p1f1	good	reasonable	0.155	0.112	0.184	0.010	-0.217	0.342	bad	reasonable	bad	**N**
MPI-ESM1-2-LR	r12i1p1f1	good	reasonable	0.159	0.125	0.181	-0.079	-0.247	0.186	bad	good	bad	**N**
MPI-ESM1-2-LR	r13i1p1f1	good	reasonable	0.141	0.101	0.162	-0.075	-0.229	0.166	reasonable	good	reasonable	**N**
MPI-ESM1-2-LR	r14i1p1f1	good	reasonable	0.147	0.110	0.175	-0.148	-0.488	0.048	bad	good	bad	**N**
MPI-ESM1-2-LR	r16i1p1f1	good	reasonable	0.167	0.134	0.188	-0.173	-0.343	0.046	bad	good	bad	**N**
MPI-ESM1-2-LR	r17i1p1f1	good	reasonable	0.165	0.129	0.187	-0.012	-0.285	0.300	bad	reasonable	bad	**N**
MPI-ESM1-2-LR	r19i1p1f1	good	reasonable	0.138	0.105	0.161	-0.251	-0.466	-0.046	reasonable	good	reasonable	**N**
MPI-ESM1-2-LR	r1i1p1f1	good	reasonable	0.172	0.133	0.205	-0.374	-0.760	-0.243	bad	good	bad	**Y**
MPI-ESM1-2-LR	r20i1p1f1	good	reasonable	0.157	0.124	0.181	-0.122	-0.334	0.108	bad	good	bad	**N**
MPI-ESM1-2-LR	r22i1p1f1	good	reasonable	0.181	0.136	0.210	-0.170	-0.376	0.008	bad	good	bad	**N**
MPI-ESM1-2-LR	r23i1p1f1	good	reasonable	0.208	0.151	0.252	-0.157	-0.690	0.171	bad	good	bad	**N**
MPI-ESM1-2-LR	r24i1p1f1	good	reasonable	0.135	0.109	0.157	-0.112	-0.308	0.106	reasonable	good	reasonable	**N**
MPI-ESM1-2-LR	r25i1p1f1	good	reasonable	0.170	0.135	0.198	-0.112	-0.502	0.087	bad	good	bad	**N**
MPI-ESM1-2-LR	r26i1p1f1	good	reasonable	0.167	0.119	0.198	-0.281	-0.688	0.048	bad	good	bad	**N**
MPI-ESM1-2-LR	r27i1p1f1	good	reasonable	0.181	0.137	0.217	-0.394	-0.663	-0.162	bad	good	bad	**N**
MPI-ESM1-2-LR	r28i1p1f1	good	reasonable	0.227	0.182	0.265	-0.255	-0.610	-0.070	bad	good	bad	**N**
MPI-ESM1-2-LR	r29i1p1f1	good	reasonable	0.170	0.141	0.193	-0.272	-0.652	-0.110	bad	good	bad	**N**
MPI-ESM1-2-LR	r2i1p1f1	good	reasonable	0.197	0.150	0.233	-0.217	-0.625	0.007	bad	good	bad	**N**
MPI-ESM1-2-LR	r30i1p1f1	good	reasonable	0.126	0.092	0.147	0.136	-0.061	0.493	reasonable	reasonable	reasonable	**N**
MPI-ESM1-2-LR	r32i1p1f1	good	reasonable	0.152	0.126	0.172	-0.208	-0.477	-0.041	bad	good	bad	**N**
MPI-ESM1-2-LR	r33i1p1f1	good	reasonable	0.164	0.132	0.185	-0.121	-0.345	0.070	bad	good	bad	**N**
MPI-ESM1-2-LR	r34i1p1f1	good	reasonable	0.188	0.152	0.224	-0.151	-0.480	0.061	bad	good	bad	**N**
MPI-ESM1-2-LR	r35i1p1f1	good	reasonable	0.155	0.115	0.179	0.069	-0.087	0.332	bad	reasonable	bad	**N**
MPI-ESM1-2-LR	r36i1p1f1	good	reasonable	0.180	0.148	0.206	-0.153	-0.365	-0.013	bad	good	bad	**N**

MPI-ESM1-2-LR	r37i1p1f1	good	reasonable	0.164	0.125	0.192	-0.310	-0.514	-0.149	bad	good	bad	**N**
MPI-ESM1-2-LR	r38i1p1f1	good	reasonable	0.174	0.143	0.201	-0.356	-0.748	-0.210	bad	good	bad	**N**
MPI-ESM1-2-LR	r39i1p1f1	good	reasonable	0.167	0.122	0.192	-0.027	-0.260	0.337	bad	reasonable	bad	**N**
MPI-ESM1-2-LR	r3i1p1f1	good	reasonable	0.137	0.102	0.169	0.064	-0.301	0.411	reasonable	reasonable	reasonable	**N**
MPI-ESM1-2-LR	r40i1p1f1	good	reasonable	0.182	0.137	0.216	-0.071	-0.398	0.308	bad	good	bad	**N**
MPI-ESM1-2-LR	r41i1p1f1	good	reasonable	0.151	0.110	0.183	-0.030	-0.400	0.308	bad	reasonable	bad	**N**
MPI-ESM1-2-LR	r42i1p1f1	good	reasonable	0.154	0.099	0.185	0.018	-0.206	0.580	reasonable	reasonable	reasonable	**N**
MPI-ESM1-2-LR	r43i1p1f1	good	reasonable	0.179	0.126	0.209	-0.117	-0.318	0.165	bad	good	bad	**N**
MPI-ESM1-2-LR	r44i1p1f1	good	reasonable	0.166	0.125	0.192	0.070	-0.099	0.285	bad	reasonable	bad	**N**
MPI-ESM1-2-LR	r45i1p1f1	good	reasonable	0.192	0.145	0.222	-0.192	-0.387	-0.034	bad	good	bad	**N**
MPI-ESM1-2-LR	r46i1p1f1	good	reasonable	0.164	0.122	0.192	-0.209	-0.422	0.024	bad	good	bad	**N**
MPI-ESM1-2-LR	r47i1p1f1	good	reasonable	0.197	0.153	0.229	-0.159	-0.456	0.028	bad	good	bad	**N**
MPI-ESM1-2-LR	r48i1p1f1	good	reasonable	0.147	0.109	0.171	-0.297	-0.462	-0.044	reasonable	good	reasonable	**N**
MPI-ESM1-2-LR	r49i1p1f1	good	reasonable	0.170	0.132	0.199	-0.455	-0.668	-0.288	bad	good	bad	**N**
MPI-ESM1-2-LR	r4i1p1f1	good	reasonable	0.121	0.082	0.151	0.221	-0.167	0.696	reasonable	reasonable	reasonable	**N**
MPI-ESM1-2-LR	r50i1p1f1	good	reasonable	0.180	0.143	0.210	-0.330	-0.574	-0.188	bad	good	bad	**N**
MPI-ESM1-2-LR	r5i1p1f1	good	reasonable	0.161	0.126	0.186	-0.212	-0.415	-0.028	bad	good	bad	**N**
MPI-ESM1-2-LR	r6i1p1f1	good	reasonable	0.181	0.128	0.228	-0.189	-0.661	0.125	bad	good	bad	**N**
MPI-ESM1-2-LR	r7i1p1f1	good	reasonable	0.190	0.152	0.216	-0.146	-0.416	0.173	bad	good	bad	**N**
MPI-ESM1-2-LR	r8i1p1f1	good	reasonable	0.169	0.136	0.196	-0.360	-0.667	-0.105	bad	good	bad	**N**
MPI-ESM1-2-LR	r9i1p1f1	good	reasonable	0.167	0.136	0.189	-0.141	-0.456	0.069	bad	good	bad	**N**
MRI-ESM2-0	r1i1p1f1	good	good	0.215	0.156	0.261	0.126	-0.115	0.428	bad	reasonable	bad	**N**
CNRM-CM6-1-HR	r1i1p1f2	good	good	0.091	0.064	0.110	-0.636	-0.849	-0.428	good	bad	bad	**Y**
CNRM-CM6-1	r1i1p1f2	good	reasonable	0.081	0.063	0.094	-0.388	-0.565	-0.262	good	good	reasonable	**Y**
EC-Earth3P-HR	r1i1p1f1	good	good	0.08674 464903	0.0814 64184 6	0.0912 49559	-0.0854 1416759	-0.137 74235 13	-0.037 06593 499	good	good	good	**N**
EC-Earth3P-HR	r2i1p1f1	good	good	0.07936 10298	0.0564 46591 09	0.0950 11504 59	-0.09110 816072	-0.323 59943 9	0.1313 19318 9	good	good	good	**Y**
EC-Earth3P-HR	r3i1p1f1	good	good	0.05862 99077	0.0477 116210 7	0.0684 61896 8	-0.4086 354994	-0.808 30954 45	-0.286 22096 41	good	good	good	**N**
EC-Earth3P	r1i1p1f1	good	good	0.091	0.064	0.110	-0.636	-0.849	-0.428	good	bad	bad	**Y**
EC-Earth3P	r2i1p1f1	good	good	0.064	0.051	0.073	-0.142	-0.324	0.092	good	good	good	**N**
EC-Earth3P	r3i1p1f1	good	good	0.076	0.057	0.087	-0.329	-0.603	-0.151	good	good	good	**N**
HadGEM3-GC31-HM	r1i1p1f1	good	good	0.071	0.052	0.081	-0.133	-0.337	0.096	good	good	good	**Y**
HadGEM3-GC31-HM	r1i2p1f1	good	good	0.073	0.056	0.085	-0.423	-0.792	-0.157	good	good	good	**N**
HadGEM3-GC31-HM	r1i3p1f1	good	good	0.070	0.057	0.082	-0.174	-0.390	-0.031	good	good	good	**N**
HadGEM3-GC31-LM	r1i1p1f1	good	reasonable	0.087	0.065	0.099	-0.239	-0.424	0.037	good	good	reasonable	**N**
HadGEM3-GC31-MM	r1i1p1f1	good	good	0.085	0.049	0.106	-0.264	-0.485	0.109	good	good	good	**N**
HadGEM3-GC31-MM	r1i2p1f1	good	good	0.075	0.057	0.089	-0.347	-0.628	-0.168	good	good	good	**Y**

HadGEM3-GC31-MM	r1i3p1f1	good	good	0.100	0.082	0.114	-0.251	-0.520	-0.111	good	good	good	**N**

Table S4: Model evaluation for FWI95 – Chilean Temperate Forest and Matorral. Evaluation results of the climate models considered for attribution analysis of FWI95 in the Chilean Temperate Forest and Matorral region. For each model, the best estimates of the Scale and Shape parameters of the GEV are shown, along with 95% confidence intervals. If the best estimate of these parameters falls within the 95% CI for the reanalysis, the model was evaluated as good; else if the 95% CIs of the model and reanalysis overlapped it was rated as reasonable; and otherwise was rated as a bad representation of the extreme FWI95 distribution. Furthermore evaluation of the seasonal cycle and spatial pattern are shown, which were evaluated by visual comparison of the seasonal and geospatial climatology to reanalysis patterns – comparison figures available on zenodo. The lowest realisation member of each model with all "good" ratings was included in the final analysis, if there was no realisation meeting that criteria, the lowest overall "reasonable" model was included.

				Sigma parameter Obs Min: 0.0734 Obs Max: 0.142			**Shape parameter Obs Min: -0.890 Obs Max: -0.269**						
Model	**Member**	**Seasonal cycle**	**Spatial pattern**	Best estimate	Lower bound	Upper bound	Best estimate	Lower bound	Upper bound	**Sigma**	**Shape**	**Rating**	**Model Inclusion**
AWI-ESM-1-REcoM	r1i1p1f1	good	reasonable	0.054	0.042	0.061	-0.612	-0.865	-0.267	reasonable	good	reasonable	**Y**
CanESM5	r1i1p2f1	good	reasonable	0.051	0.037	0.061	-0.352	-0.706	-0.132	bad	good	bad	**Y**
CanESM5	r8i1p1f1	good	reasonable	0.068	0.053	0.081	-0.430	-0.719	-0.279	good	good	reasonable	**N**
CNRM-CM6-1-HR	r1i1p1f2	good	good	0.077	0.063	0.088	-0.661	-0.891	-0.441	good	good	good	**N**
CNRM-CM6-1	r1i1p1f2	good	reasonable	0.061	0.051	0.068	-0.362	-0.654	-0.264	reasonable	good	reasonable	**N**
CNRM-ESM2-1	r1i1p1f2	good	reasonable	0.070	0.049	0.086	-0.413	-0.724	-0.208	good	good	reasonable	**Y**
GFDL-CM4	r1i1p1f1	good	reasonable	0.081	0.062	0.098	-0.569	-0.839	-0.410	good	good	reasonable	**Y**
INM-CM4-8	r1i1p1f1	good	bad, central south too firey	0.051	0.040	0.058	-0.194	-0.480	-0.032	bad	bad	bad	**N**
INM-CM5-0	r1i1p1f1	good	bad, central south too firey	0.055	0.042	0.063	-0.240	-0.551	0.041	reasonable	bad	bad	**N**
MIROC6	r1i1p1f1	good	reasonable	0.056	0.044	0.067	-0.717	-0.926	-0.547	reasonable	good	reasonable	**N**
MIROC6	r2i1p1f1	good	reasonable	0.087	0.061	0.104	-0.572	-0.765	-0.350	good	good	reasonable	**Y**
MIROC6	r3i1p1f1	good	reasonable	0.061	0.046	0.073	-0.428	-0.688	-0.287	good	good	reasonable	**N**
MPI-ESM1-2-LR	r10i1p1f1	good	reasonable	0.061	0.048	0.071	-0.378	-0.600	-0.177	good	good	reasonable	**N**
MPI-ESM1-2-LR	r11i1p1f1	good	reasonable	0.039	0.031	0.045	-0.192	-0.484	-0.052	bad	bad	bad	**N**
MPI-ESM1-2-LR	r12i1p1f1	good	reasonable	0.061	0.045	0.072	-0.431	-0.653	-0.278	good	good	reasonable	**N**
MPI-ESM1-2-LR	r13i1p1f1	good	reasonable	0.051	0.036	0.062	-0.366	-0.645	-0.191	reasonable	good	reasonable	**N**
MPI-ESM1-2-LR	r14i1p1f1	good	reasonable	0.047	0.038	0.053	-0.243	-0.525	-0.100	bad	bad	bad	**N**
MPI-ESM1-2-LR	r15i1p1f1	good	reasonable	0.053	0.039	0.064	-0.438	-0.685	-0.263	reasonable	good	reasonable	**N**
MPI-ESM1-2-LR	r16i1p1f1	good	reasonable	0.043	0.034	0.051	-0.528	-0.798	-0.378	bad	good	bad	**N**
MPI-ESM1-2-LR	r17i1p1f1	good	reasonable	0.059	0.044	0.070	-0.487	-0.775	-0.214	reasonable	good	reasonable	**N**
MPI-ESM1-2-LR	r18i1p1f1	good	reasonable	0.065	0.051	0.078	-0.627	-0.878	-0.455	good	good	reasonable	**N**
MPI-ESM1-2-LR	r19i1p1f1	good	reasonable	0.065	0.043	0.078	-0.461	-0.667	-0.222	good	good	reasonable	**N**
MPI-ESM1-2-LR	r1i1p1f1	good	reasonable	0.053	0.040	0.063	-0.363	-0.673	-0.252	reasonable	good	reasonable	**Y**
MPI-ESM1-2-LR	r20i1p1f1	good	reasonable	0.050	0.040	0.058	-0.186	-0.345	-0.038	bad	bad	bad	**N**
MPI-ESM1-2-LR	r21i1p1f1	good	reasonable	0.053	0.042	0.063	-0.180	-0.411	0.003	reasonable	bad	bad	**N**

MPI-ESM1-2-LR	r22i1p1f1	good	reasonable	0.057	0.036	0.069	-0.366	-0.590	-0.070	reasonable	good	reasonable	**N**
MPI-ESM1-2-LR	r23i1p1f1	good	reasonable	0.063	0.049	0.073	-0.373	-0.578	-0.212	good	good	reasonable	**N**
MPI-ESM1-2-LR	r24i1p1f1	good	reasonable	0.057	0.044	0.067	-0.505	-0.742	-0.289	reasonable	good	reasonable	**N**
MPI-ESM1-2-LR	r25i1p1f1	good	reasonable	0.050	0.040	0.059	-0.281	-0.608	-0.028	bad	bad	bad	**N**
MPI-ESM1-2-LR	r26i1p1f1	good	reasonable	0.046	0.036	0.053	-0.248	-0.443	-0.090	bad	bad	bad	**N**
MPI-ESM1-2-LR	r27i1p1f1	good	reasonable	0.049	0.031	0.059	-0.278	-0.566	0.303	bad	reasonable	bad	**N**
MPI-ESM1-2-LR	r28i1p1f1	good	reasonable	0.042	0.034	0.048	-0.187	-0.360	-0.032	bad	bad	bad	**N**
MPI-ESM1-2-LR	r29i1p1f1	good	reasonable	0.067	0.055	0.077	-0.496	-0.718	-0.313	good	good	reasonable	**N**
MPI-ESM1-2-LR	r2i1p1f1	good	reasonable	0.048	0.032	0.060	-0.662	-0.875	-0.354	bad	good	bad	**N**
MPI-ESM1-2-LR	r30i1p1f1	good	reasonable	0.049	0.040	0.057	-0.424	-0.703	-0.295	bad	good	bad	**N**
MPI-ESM1-2-LR	r31i1p1f1	good	reasonable	0.044	0.033	0.053	-0.257	-0.544	-0.031	bad	bad	bad	**N**
MPI-ESM1-2-LR	r32i1p1f1	good	reasonable	0.046	0.035	0.054	-0.237	-0.436	-0.044	bad	bad	bad	**N**
MPI-ESM1-2-LR	r33i1p1f1	good	reasonable	0.057	0.043	0.067	-0.336	-0.507	-0.152	reasonable	bad	bad	**N**
MPI-ESM1-2-LR	r34i1p1f1	good	reasonable	0.038	0.026	0.051	-0.231	-0.775	0.189	bad	reasonable	bad	**N**
MPI-ESM1-2-LR	r35i1p1f1	good	reasonable	0.053	0.038	0.064	-0.315	-0.568	-0.063	reasonable	bad	bad	**N**
MPI-ESM1-2-LR	r36i1p1f1	good	reasonable	0.054	0.043	0.063	-0.359	-0.645	-0.220	reasonable	good	reasonable	**N**
MPI-ESM1-2-LR	r37i1p1f1	good	reasonable	0.063	0.050	0.076	-0.420	-0.712	-0.249	good	good	reasonable	**N**
MPI-ESM1-2-LR	r38i1p1f1	good	reasonable	0.051	0.039	0.061	-0.621	-0.872	-0.404	reasonable	good	reasonable	**N**
MPI-ESM1-2-LR	r39i1p1f1	good	reasonable	0.047	0.038	0.054	-0.145	-0.449	0.008	bad	bad	bad	**N**
MPI-ESM1-2-LR	r3i1p1f1	good	reasonable	0.048	0.038	0.056	-0.534	-0.805	-0.330	bad	good	bad	**N**
MPI-ESM1-2-LR	r40i1p1f1	good	reasonable	0.058	0.045	0.066	-0.668	-0.897	-0.319	reasonable	good	reasonable	**N**
MPI-ESM1-2-LR	r41i1p1f1	good	reasonable	0.048	0.034	0.058	-0.426	-0.775	-0.081	bad	good	bad	**N**
MPI-ESM1-2-LR	r42i1p1f1	good	reasonable	0.049	0.039	0.059	-0.443	-0.777	-0.231	bad	good	bad	**N**
MPI-ESM1-2-LR	r43i1p1f1	good	reasonable	0.046	0.038	0.053	-0.385	-0.676	-0.148	bad	good	bad	**N**
MPI-ESM1-2-LR	r44i1p1f1	good	reasonable	0.042	0.030	0.050	-0.151	-0.469	0.061	bad	reasonable	bad	**N**
MPI-ESM1-2-LR	r45i1p1f1	good	reasonable	0.046	0.036	0.056	-0.239	-0.598	-0.037	bad	bad	bad	**N**
MPI-ESM1-2-LR	r46i1p1f1	good	reasonable	0.046	0.036	0.052	-0.341	-0.591	-0.064	bad	bad	bad	**N**
MPI-ESM1-2-LR	r47i1p1f1	good	reasonable	0.046	0.034	0.055	-0.223	-0.396	-0.016	bad	bad	bad	**N**
MPI-ESM1-2-LR	r48i1p1f1	good	reasonable	0.057	0.043	0.065	-0.551	-0.758	-0.238	reasonable	good	reasonable	**N**
MPI-ESM1-2-LR	r49i1p1f1	good	reasonable	0.061	0.047	0.073	-0.492	-0.793	-0.336	good	good	reasonable	**N**
MPI-ESM1-2-LR	r4i1p1f1	good	reasonable	0.041	0.033	0.047	-0.197	-0.391	-0.025	bad	bad	bad	**N**
MPI-ESM1-2-LR	r50i1p1f1	good	reasonable	0.058	0.047	0.067	-0.498	-0.767	-0.293	reasonable	good	reasonable	**N**
MPI-ESM1-2-LR	r5i1p1f1	good	reasonable	0.057	0.045	0.067	-0.677	-0.867	-0.447	reasonable	good	reasonable	**N**
MPI-ESM1-2-LR	r6i1p1f1	good	reasonable	0.052	0.039	0.062	-0.472	-0.731	-0.315	reasonable	good	reasonable	**N**
MPI-ESM1-2-LR	r7i1p1f1	good	reasonable	0.053	0.042	0.062	-0.616	-0.862	-0.336	reasonable	good	reasonable	**N**
MPI-ESM1-2-LR	r8i1p1f1	good	reasonable	0.055	0.043	0.064	-0.365	-0.600	-0.212	reasonable	good	reasonable	**N**
MPI-ESM1-2-LR	r9i1p1f1	good	reasonable	0.04586330903	0.03563839521	0.05365611964	-0.344885468	-0.69165368 37	-0.19123891 64	bad	bad	bad	**N**
MRI-ESM2-0	r1i1p1f1	good	reasonable	0.10860 95373	0.08675606376	0.12623203 84	-0.5781 168461	-0.833 211174 2	-0.378 36432 4	reasonable	good	reasonable	**Y**
CNRM-CM6-1-HR	r1i1p1f2	good	good	0.07168 843287	0.05610196835	0.0828 29934 99	-0.6990 054566	-0.925 01074	-0.422 22998 45	good	good	good	**N**

CNRM-CM6-1	r1i1p1f2	good	reasonable	0.070	0.046	0.088	-0.466	-0.662	-0.131	good	good	reasonable	**Y**
EC-Earth3P-HR	r1i1p1f1	good	good	0.058	0.055	0.061	-0.342	-0.389	-0.299	bad	bad	bad	**N**
EC-Earth3P-HR	r2i1p1f1	good	good	0.066	0.046	0.081	-0.327	-0.615	-0.102	good	bad	bad	**Y**
EC-Earth3P-HR	r3i1p1f1	good	good	0.059	0.046	0.069	-0.181	-0.337	-0.005	reasonable	bad	bad	**N**
EC-Earth3P	r1i1p1f1	good	good	0.062	0.059	0.065	-0.334	-0.379	-0.288	good	bad	bad	**Y**
EC-Earth3P	r2i1p1f1	good	good	0.059	0.047	0.068	-0.315	-0.479	-0.161	reasonable	bad	bad	**N**
EC-Earth3P	r3i1p1f1	good	good	0.058	0.042	0.069	-0.421	-0.727	-0.078	reasonable	good	reasonable	**N**
HadGEM3-GC31-HM	r1i1p1f1	good	good	0.048	0.036	0.056	-0.511	-0.747	-0.283	bad	good	bad	**N**
HadGEM3-GC31-HM	r1i2p1f1	good	good	0.049	0.040	0.057	-0.289	-0.653	-0.174	bad	bad	bad	**N**
HadGEM3-GC31-HM	r1i3p1f1	good	good	0.057	0.038	0.069	-0.481	-0.706	-0.183	reasonable	good	reasonable	**Y**
HadGEM3-GC31-LM	r1i1p1f1	good	bad	0.044	0.029	0.052	-0.733	-0.954	-0.333	bad	good	bad	**N**
HadGEM3-GC31-MM	r1i1p1f1	good	reasonable	0.05450275773	0.04012681 82	0.065368974 57	-0.5394866444	-0.75042716 74	-0.36571799 98	reasonable	good	reasonable	**Y**
HadGEM3-GC31-MM	r1i2p1f1	good	reasonable	0.0575118544	0.04590591 494	0.068886372 31	-0.5560316181	-0.91219489 22	-0.44860114 93	reasonable	good	reasonable	**N**
HadGEM3-GC31-MM	r1i3p1f1	good	reasonable	0.05973510293	0.04595850 706	0.070603386 38	-0.3456996065	-0.51912890 65	-0.19476691 75	reasonable	bad	bad	**N**

As described in both the 2023-24 and 2024-25 reports, a baseline period of 1960-2013 was utilised for the HadGEM3-A attribution analysis. The 2025-26 report reduces this baseline period to 1980-2013 due to the uncertainties inherent to the pre-satellite era of reanalysis products, in particular in ERA5. As stated in the final back-extension to 1940 specification; 'Trends in 2-m temperature anomalies over land for ERA5, both globally and over Europe, show generally excellent agreement with independent datasets based entirely on surface observations, particularly for the late 1970s onwards (Soci et al., 2024). Given the importance of 2-m temperature in various stages of the FWI calculation, along with poor wind field representation, the baseline period start was moved forward from 1960 to 1980. A 33 year baseline (1980-2013) is consistent with typical climatology periods of 30 years. This baseline period gives not only relevant context for the event values of FWI to past years, but is used to perform bias adjustment of the HadGEM3-A large attribution ensemble ('Attribution Ensemble'). This ensemble of 525 members is run twice, once with natural only forcings from solar variability and volcanic activity (Counterfactual) and one including anthropogenic emissions (Factual). As discussed individually in **Sections S3, S4 and S5**, the HadGEM3-A historical ensemble ('Historical Ensemble'), which is the 15-member counterpart run over the period 1960-2013 used to evaluate model performance, tends to overestimate the FWI95 value with respect to reanalysis observations in the focal regions. By applying a trend-preserving linear regression based on the historical ensemble and anchored to each year of the 2020-2024 ensemble, an effective 39,375-member attribution ensemble can be generated for both the natural and anthropogenically altered climate simulations. Bootstrapping the FWI95 value for each year 10,000 times allows for a high confidence range for the Probability Ratio to be calculated. Importantly, due to improvements in distributed processing, a mixture of methods was used to convert the raw input variables (Daily total precipitation, t2m, daily mean wind speed, daily mean relative humidity) into the daily FWI values. ERA5 and the HadGEM3-A large attribution ensemble were processed using the xclim library while the HadGEM3-A historical ensemble was processed using the ImpactsToolBox, consistent with the method described in previous reports. Efforts are being made to migrate the entire process over to an xclim framework, similar to the one used by WWA. The reasoning for a mixed methodology involving a portion processed using the

ImpactsToolBox and another portion processed using xclim is the addition of xclim allowed for the entirety of the HadGEM3-A large attribution ensemble to be utilised, enabling all 525 members to be used for calculation of the attribution statements. Until the xclim based method has been validated on the Historical Ensemble, relying on the previously validated method is a reasonable compromise. Agreement between ERA5 and attribution ensemble values for the FWI between xclim and the ImpactsToolBox methods allow for the faster method to be substituted in with no significant change to downstream results. WWA uses the xclim library for FWI calculations used in the reanalysis, model and synthesis results.

For the three different model analyses included in this report, slightly different variables were used for the calculation of FWI. While all use maximum daily temperature and total daily precipitation, the WWA multi-model approach uses minimum relative humidity and maximum wind speed, the HadGEM3-A large ensemble is calculated using mean relative humidity and mean wind speed, and the CMIP6 ensemble analysis uses minimum relative humidity and mean wind speed. These differences are unlikely to cause substantial changes in the results compared to the model uncertainty, but may result in larger possible ranges of PR across different metrics.

S1.2.2. Attribution of Present Day Focal Events - BA

We follow the same overall ConFLAME framework as in the previous report. ConFLAME consists of two main components: (1) a fire model describing the controls on burned area (BA), and (2) a Bayesian inference framework used to estimate model parameters and quantify uncertainty.

1) **Fire model formulation.** The fire model represents BA as the combined effect of key controls on fire activity: fuel connectivity, fuel dryness, ignitions, and anthropogenic suppression. Each control is expressed as a linear combination of its driving variables (listed in **Table S5**), transformed using a logistic function to represent its limiting effect on burning. Each control therefore describes the maximum fraction of burned area that would occur under otherwise favourable conditions. Total BA is calculated as the product of these controls, modulated by an additional term, $Q_{spread,}$ which represents variability in fire outcomes not captured by the model drivers. This includes both unresolved processes and inherent stochasticity in fire activity.

2) **Bayesian inference and uncertainty.** Model parameters are estimated using a Maximum Entropy Bayesian inference approach. This framework identifies the range of parameter values that are consistent with observed burned area, rather than a single optimal solution. As a result, the model produces a posterior distribution of parameters, which propagates through to a distribution of modelled BA outcomes.

   Q_{spread} is treated as a hierarchical parameter, meaning that it introduces additional variability conditional on the other model parameters. This allows the model to represent uncertainty arising both from parameter estimation and from unobserved variability in fire behaviour.

   The model is calibrated against MODIS burned area observations (**Sect. 2.1.2.1**). Training is conducted on a subset (10%) of the available data spanning January 2002 to February 2026, following the same inference protocol as in Kelley et al. (2025). Optimisation uses a No-U-Turns (NUTS) approach, with 1000 warm-up and 1000 sampling iterations over 10 chains. 100 samples are taken from each chain for attribution experiments.

Table S5: Predictors used by ConFLAME attribution setup. Drivers are grouped into four control categories. (+) or (–) signs representing positive or negative influence over fire occurrence in ConFLAME.

Control	***Driver***	***Directional contribution***	***Temporal resolution***	***Factual***	***Source***	***Counterfactual***
Fuel	Tree cover	+	Snapshot 2020	Fractional cover of Broadleaf and Needleleaf PFT	HadGEM3-A (Ciavarella et al., 2018)	ISAM-HYDE moderated by JULES V6.0 (Meiyappan, et al., 2012)
	Shrub cover	+		Fractional cover of Shrub		
	Herbaceous Cover	+		Fractional cover of C3 and C4 grass		
Weather	Maximum consecutive number of dry days	+	Monthly	Running mean of continuous days with precip < 0.1mm	ERA5 (Muñoz-Sabater et al., 2021)	ERA5 with climate change signal removed using difference between HadGEM3-A (Ciavarella et al., 2018) all forcings and natural only simulations
	Precipitation	–	Monthly	Monthly totals of daily precip		
	Maximum monthly temperature	+	Monthly	Maximum of daily maximums for month		
	Mean monthly minimum humidity	–	Monthly	Calculated as per Kelley et al. (2025)		
Ignition/ Suppression	Pasture Fraction	+ ignitions - suppression	Annual	Linear interpolation to a monthly timestep	HYDE (Klein Goldewijk et al., 2010)	Kept same as factual
	Cropland Fraction	+ ignitions - suppression	Annual			
	Urban Population	- suppression	Annual			
	Rural Population	+ ignitions - suppression	Annual			
	Cloud-to-ground lightning	+ ignitions	Monthly		(Qu et al. 2025)	

Attribution simulations: factual and counterfactual
For attribution, the trained model is run in predictive mode using both factual and counterfactual inputs. The factual simulations are driven by ERA5 reanalysis data (**Table S5**) and represent the real-world meteorological conditions under which the fires occurred.

The counterfactual simulations use the same underlying ERA5 data, but with the anthropogenic climate signal removed. This is achieved using the HadGEM3-A large ensemble to estimate the difference between simulations with and without anthropogenic forcing. These differences are applied to each meteorological and fuel variable to generate counterfactual conditions consistent with a world without human influence.

This approach ensures that the timing and structure of the observed event are preserved, while isolating the effect of anthropogenic climate change. Due to the temporary unavailability of HadGEM3-A simulations beyond 2024, we use ensemble members from 2021–2024 to represent the anthropogenic signal, resulting in 2100 counterfactual realisations (4 years × 525 ensemble members).

Ensemble generation
We generate 1000 paired factual and counterfactual simulations by sampling from the posterior parameter distribution. For counterfactual runs, meteorological adjustments are also randomly sampled from the available HadGEM3-A ensemble members. This produces an ensemble that captures uncertainty in both model parameters and climate forcing.

In this year's analysis, two additional constraints are introduced to improve the robustness of attribution estimates:

1. **Paired stochasticity**: Paired stochasticity: Qspread represents variability in burned area arising from factors not explicitly represented in the model, including the inherent stochasticity of fire activity. Because the aim of the attribution experiment is to isolate the influence of anthropogenic climate forcing on the observed event, we pair Qspread values between corresponding factual and counterfactual simulations. This ensures that differences between the two worlds arise from the imposed climate signal rather than random variability in fire response, analogous to the paired treatment of meteorological conditions in the factual and counterfactual forcing datasets. Stochastic variability is therefore retained within the simulations but controlled for when comparing the two worlds.
2. **Conditioning on observed burned area:** We explicitly condition the model posterior on the observed BA for the target event. This is achieved by reweighting the posterior distribution according to the likelihood of reproducing the observed BA in the factual. The likelihood term is an extension of equation 9 in Barbosa et al. (2025):

$$P\left(\beta|\left(\{BF_i\},\ \{X_{i,v}\} \cap \{BF_j\}\right)\right) \propto \prod_{j}^{event} P\left(\beta|\{BF_i\},\ \{X_{i,v}\}\right)^{BF_j} \times \left(1 - P\left(\beta|\{BF_i\},\ \{X_{i,v}\}\right)\right)^{1-BF_j}$$

Where β is our parameter set, $\{BF_i\}$ is our set of historical observed burn fractions $\{X_{i,v}\}$ the driving variables, and $\{BF_j\}$ is burned area during our focal event

This weight is also applied to the paired counterfactual, and ensures that attribution focuses on the subset of model realisations consistent with the observed event. Attribution results are derived from these reweighted posterior distributions. The amplification factor (AF) is calculated as the ratio of burned area under factual and counterfactual conditions for events of equivalent likelihood, across all re-weighted posteriors (not just the portion where factual exceeded observed, as per last year).

The probability ratio (PR) is calculated as the change in likelihood of events with comparable BA between factual and counterfactual simulations.

Uncertainty ranges (5th–95th percentiles) arise directly from the posterior ensemble and reflect both parameter uncertainty and variability in fire outcomes.

S1.2.3. Future Projections - BA

For future projections, we trained the model on ISIMIP3a GSWP3 reanalysis data and used ISIMIP3b bias-corrected GCMs to perform future projections as outlined in **Section 2.5.4**, following previous reports (Kelley et al. 2025).

ConFLAMEs uninformed priors used in previous reports included parameter combinations in which fire controls became effectively saturated. Preliminary tests this year showed that, for the smaller focal regions in this year's report, the posterior distribution did not always sufficiently constrain parts of the parameter space that implied dryness had little or no influence on burned area. This is inconsistent with the strong observational and process-based evidence that dryness conditions influence fire activity in all three focal regions (see hydroclimatic analyses in the main report). We therefore modify the update function described in Barbosa et al. (2025) by excluding parameter combinations for which the dryness control can alter the relative burned area by less than 1%. In other words, parameterisations that imply dryness changes can never modify burned area by more than 1%, regardless of the severity of the weather conditions, are assigned zero probability.

$$P\left(\{\beta_p\}|\{BF_i\},\ \{X_{i,v}\}\right) \propto P(\{\beta_p\}) \times \prod_{i}^{cell} \begin{cases} P(BF_i \mid \{\beta_p\},\ \{X_v\}) & if\ \frac{\Sigma_i f(\{X_v\}_{dryness}, \{\beta_p\}_{dryness})}{ncells} < 0.99 \\ 0 & otherwise \end{cases}$$

S1.2.4. Future Projections - Typical Fire Behaviour

Whilst the current report focuses on 2025/2026 extreme fires, the Haas et al. (2026) GLMs were derived to represent the large-scale changes in median conditions of BA, fire size and fire intensity. As such, the projections here represent simulated increases or decreases in the median fire activity. They do not simulate how the distribution will change, nor do they simulate extreme events. This analysis aimed to determine whether a clear qualitative trend could be identified for any of the focal regions of properties beyond burned area, notably fire size and fire intensity. Given that the model outputs were computed at a 50km resolution, the ability of the models to reproduce fine-scale detail is limited and the outputs remain fairly coarse relative to the region size. This introduces systematic uncertainty, as the subpixel landscape and vegetation features will not be represented accurately. Furthermore, the 2010-2020 baseline was run using simulated vegetation cover from BIOME4 (Kaplan et al., 2003) and the P-Model (Stocker et al., 2020). This means that vegetation was driven by climate drivers alone, and does not capture observed land fractions, such as plantations or human land use. Nevertheless, it provides an evaluation of the current state-of-the-art fire size and intensity global models, and highlights the need for improvement and higher resolution regional modeling.

Table S6: Evaluation of the Haas et al. (2026) GLMs

Focal region	Variable	Observations	Baseline	Bias	RMSE	Correlation	NME
Burned Area (BA) (reported as percent)							
Northwest Iberia	BA	0.075%	0.23%	0.001	0.003	0.06	3.04
Canada	BA	0.11%	0.37%	0.002	0.003	-0.11	1.32
Chile	BA	0.037%	0.24%	0.002	0.003	0.19	4.07
Fire Size (FS) km^2							
Northwest Iberia1	FS	1.78 km^2	0.33 km^2	-1.44	2.164	0.64	0.85
Canada2	FS	7.85 km^2	4.29 km^2	-3.56	11.710	0.04	0.99
Chile3	FS	3.02 km^2	0.91 km^2	-2.11	4.843	-0.04	1.04
Fire Intensity (FI) $W.km^2$							
Northwest Iberia	FI	33.64 $W.km^2$	15.83 $W.km^2$	-17.81	28.401	-0.15	1.68
Canada	FI	49.01 $W.km^2$	40.61 $W.km^2$	-8.41	74.081	-0.04	1.01
Chile	FI	30.45 $W.km^2$	23.84 $W.km^2$	-6.61	29.243	-0.07	1.27

The Haas et al. GLM demonstrates the strongest and most consistent performance in Chile and Canada, particularly for burned area and best performance in Iberia for fire size (**Table S6**). For burned area, Chile shows acceptable performance in mean prediction and correlation, with moderate spatial agreement between modelled and observed patterns (spatial correlations ~0.2) and no systematic bias. However, the normalised mean square error is very large, meaning that the amplitude of the predictions varies greatly. This may be problematic for future projections. Canada also performs reasonably well, likely reflecting the model's ability to capture large-scale climatic controls and relatively homogeneous fuel structures. There does appear to be a systematic underestimation in the north-western region. In contrast, Iberia highlights key limitations. These results suggest that burned area is sensitive to vegetation representation, particularly in heterogeneous landscapes. Improving fuel and vegetation detail, as well as training or running the model at higher spatial resolution, could substantially improve performance in regions like Iberia. Fire size broadly follows the same regional performance patterns as burned area, with strong skill in Iberia, Chile and Canada and weaker performance in more heterogeneous regions. However, fire size is more strongly governed by fuel-related factors, particularly fuel continuity and fragmentation (e.g. landscape structure, roads, agricultural boundaries) which tend to be more stable in both present-day and projected future conditions. This relative stability in fuel fragmentation patterns may contribute to more consistent predictions in fire size compared to fire intensity, although projection confidence remains moderate and region-dependent. Fire intensity is the most challenging variable for the model to capture.

The model is highly sensitive to long-term drought effects, particularly through its influence on vegetation and fuel accumulation. In the current setup, reduced seasonal fuel accumulation under prolonged drought leads to declining projected fire intensity, which may not fully reflect real-world dynamics where drought can also increase flammability. Fire intensity projections carry greater uncertainty than burned area and fire size. This uncertainty highlights that fire intensity responses to drought are likely region-dependent and poorly captured in the current modelling framework. This reflects both limitations in representing vegetation processes and their interaction with long-term dryness, and the challenge of resolving fine-scale variability at larger model scales. In Chile, there are also somewhat promising signals in fire intensity, although performance for intensity is consistently weaker than for the other two metrics. Across all regions, model skill varies depending on the fire characteristic being assessed, reflecting differences in the dominant controls on burned area, fire size, and intensity.

S2. Global Extreme Wildfire Events of 2025-26

S2.1. Supplementary Analysis: Cross-Product Intercomparison of Regional Burned Area Totals

To characterise the dependence of our findings on BA product choices, we add a supplementary comparison between the regional BA totals detected by the MCD64A1 BA product and two other BA products (**Figure S1**). The first comparison product was the ESA Climate Change Initiative Harmonised Medium Resolution Burned Area Grid product version 6.0 (MRBA60H). MRBA60 is a new harmonised global burned area dataset that extends the ESA FireCCI record from 2003 to the present at monthly 0.25° resolution. From 2019 onwards, MRBA60 uses the FireCCIS311 (Lizundia-Loiola et al., 2022) grid product directly, which is derived from Sentinel-3 SYN surface reflectance, combining OLCI and SLSTR reflectance, and guided by VIIRS active fire detections through a contextual algorithm at 300 m resolution. For 2003-2018, MRBA60 is based on the long-term MODIS-derived FireCCI51 record (Lizundia-Loiola et al., 2020), but uses biome and season specific Random Forest models to predict burned area values harmonised with the higher resolution Sentinel-3 based FireCCIS311 product. These models were trained over the 2019-2024 overlap between FireCCI51 and FireCCIS311, with additional predictors including active fires, fire radiative power, climate and vegetation indices (Torres-Vazquez et al., 2026). The second comparison product is NASA's VIIRS BA product (VNP64A1 v002; Giglio et al., 2025), generated using an adaptation of the MODIS MCD64A1 Collection 6.1 algorithm, applied to 750 m VIIRS imagery and active fire detections. The hybrid algorithm uses dynamic thresholds on composite imagery derived from a burn-sensitive vegetation index and temporal texture measures, enabling it to distinguish fire-induced changes from other land surface changes. It identifies the burn date at 500 m resolution for each grid cell, with prior probabilities of burned/unburned areas informed by cumulative VIIRS active fire observations.

The VIIRS VNP64A1 product has been available since 2013 only, and hence our cross-product comparisons focus on the fire seasons March 2013-February 2026. We followed identical approaches as described in **Section 2.1.2** to calculate regional BA totals and to quantify anomalies of the past fire season.

With very few exceptions, we find a high level of consistency between the MCD64A1, FireCCIS311, and VIIRS VNP64A1 BA products with regards to both the relative magnitude of regional BA anomalies, the geographical distribution of those anomalies, and the rankings of BA in the 2025-26 fire season versus previous fire seasons since 2019 (**Figure S1**). This analysis adds confidence that regional anomalies identified in the MCD64A1 BA product are consistent across products from different space agencies using different algorithms applied to different combinations of Earth-observing sensors. The MCD64A1 BA product will soon discontinue due to the decommissioning of MODIS sensors aboard NASA's Terra and Aqua satellites, and the consistency across products is an encouraging finding for the continuity of our annual reporting.

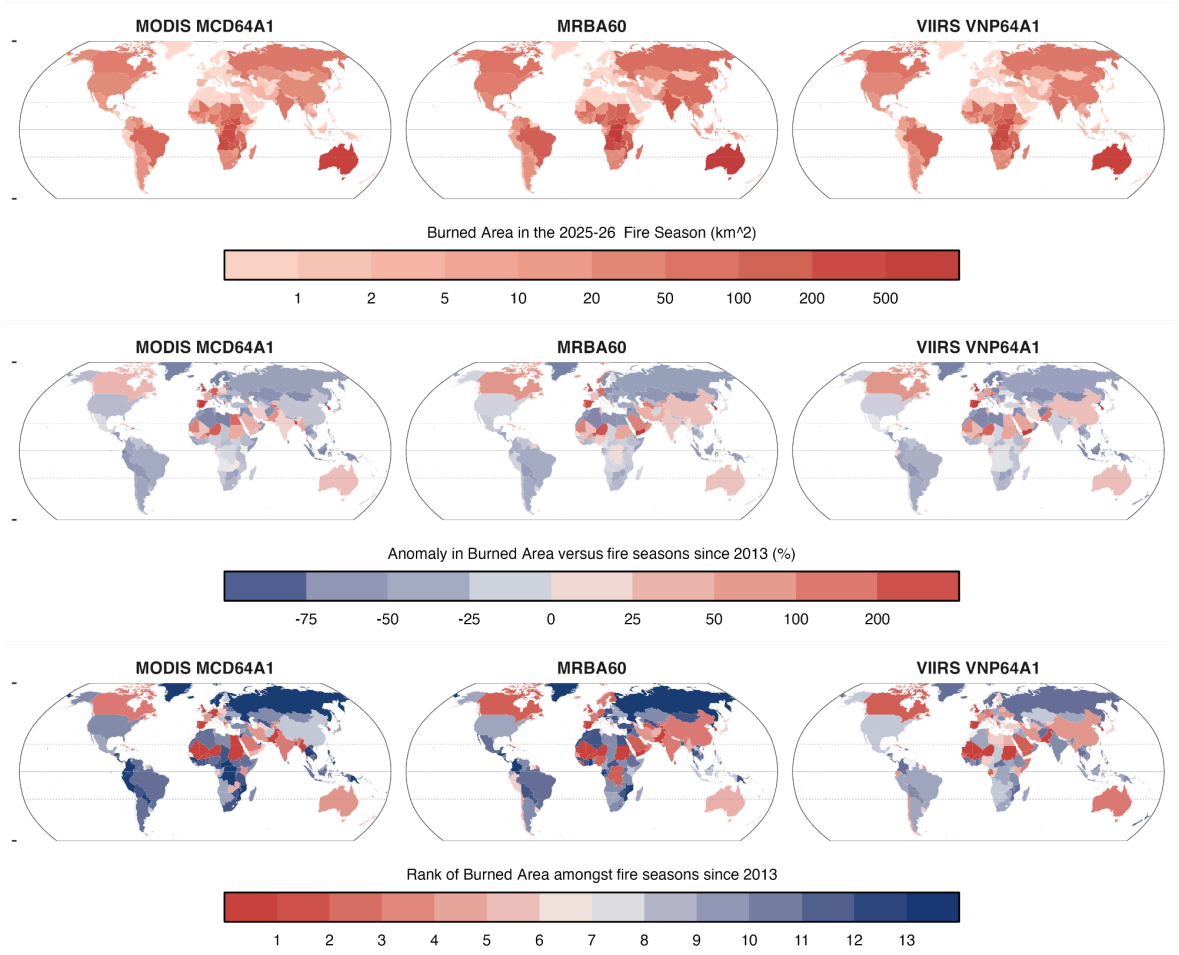


Figure S1: Comparison of the burned area (BA) estimates from **(left column)** the ESA Climate Change Initiative FireCCI Harmonised Medium Resolution Burned Area Grid product version 6.0 (MRBA60H; Torres-Vazquez et al., 2026), **(middle column)** the VIIRS BA product produced by NASA (VNP64A1 v002) (Giglio, 2024; Zubkova et al., 2024) and **(right column)** the MODIS BA product produced by NASA (MCD64A1 collection 6.1; Giglio et al., 2018).

S2.2. Supplementary Analysis: Contemporaneous Extremes in Fire Weather

As in last year's report, we produce routine summaries of the extreme (95th percentile) fire weather days during the March 2025-February 2026 global fire season based on the FWI, a common metric of fire danger developed by the Canadian Forest Service as part of the Canadian Forest Fire Danger Rating System (CFFDRS; van Wagner, 1987). The FWI comprises various components that consider the influence of weather on fire danger, with 2m temperature, 10m wind speed, precipitation, and 2m relative humidity as prerequisite variables. Higher FWI values are generally seen during droughts, heatwaves and strong winds as these conditions are conducive to wildfires in environments with sufficient fuel load (Jolly et al., 2015; Di Giuseppe, 2016; Jones et al., 2022). We base our analysis of extreme (95th percentile) fire weather on the FWI dataset derived from the Copernicus Climate Change Service ERA5 reanalysis (Hersbach et al., 2020; Vitolo et al., 2020) and maintained by the Copernicus Emergency Management Service (CEMS, version 4.1, 2019). The 95th percentile value for extreme fire weather has been used in many prior publications (e.g., Abatzoglou et al., 2019; Jones et al., 2022). The same statistics are reported for the 2025-26 fire season as in the case of fire observational datasets, including (i) ranks, (ii) proportional anomalies, and (iii) standardised anomalies amongst all fire seasons since 2002 (**Figure S2**).

We no longer comment at length on the results of this analysis, but recognise that the data may be of value to certain end users. The data produced using these methods are available from Turco et al. (2026).

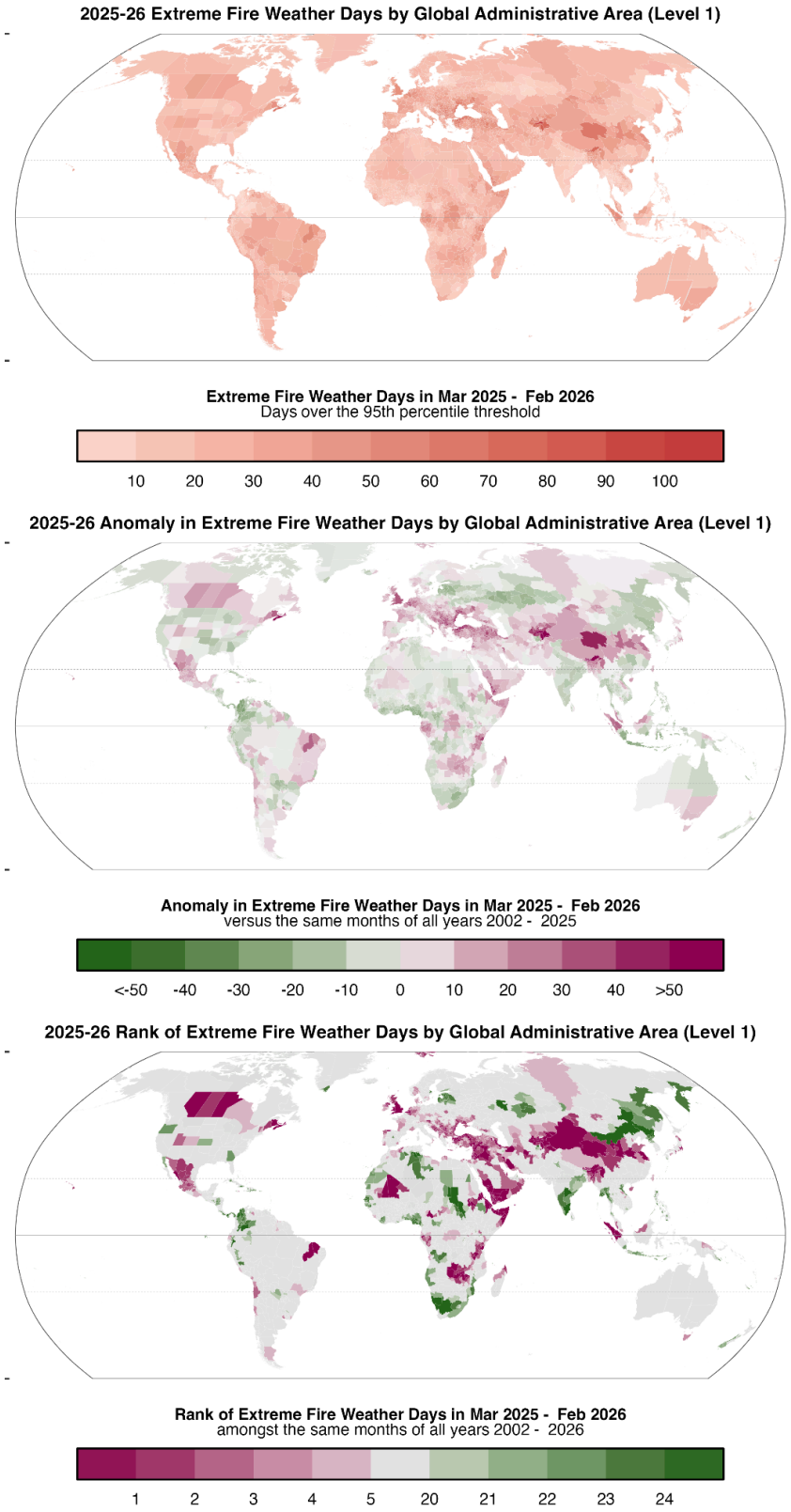


Figure S2: Extreme fire weather in the past fire season, including **(top panel)** the number of days with extreme (95th percentile) fire weather during the 2025-26 fire season, **(middle panel)** the anomaly versus the mean of all prior fire seasons 2002-2025, and **(bottom panel)** rank amongst all fire seasons since 2002.

S2.3. Supplementary Analysis: 21st Century Trends in Burned Area

To place recent extremes in the context of fire trends of the past two decades, we update our regional analyses of trends in annual BA from Jones et al. (2022). In addition to reporting trends in *total* BA, we also present trends in *forest* BA as these regularly diverge from total BA trends (**Figure S3**), following Jones et al. (2024a).

We no longer comment at length on the results of this analysis, but recognise that the data may be of value to certain end users. The data produced using these methods are available from Jones et al. (2026).

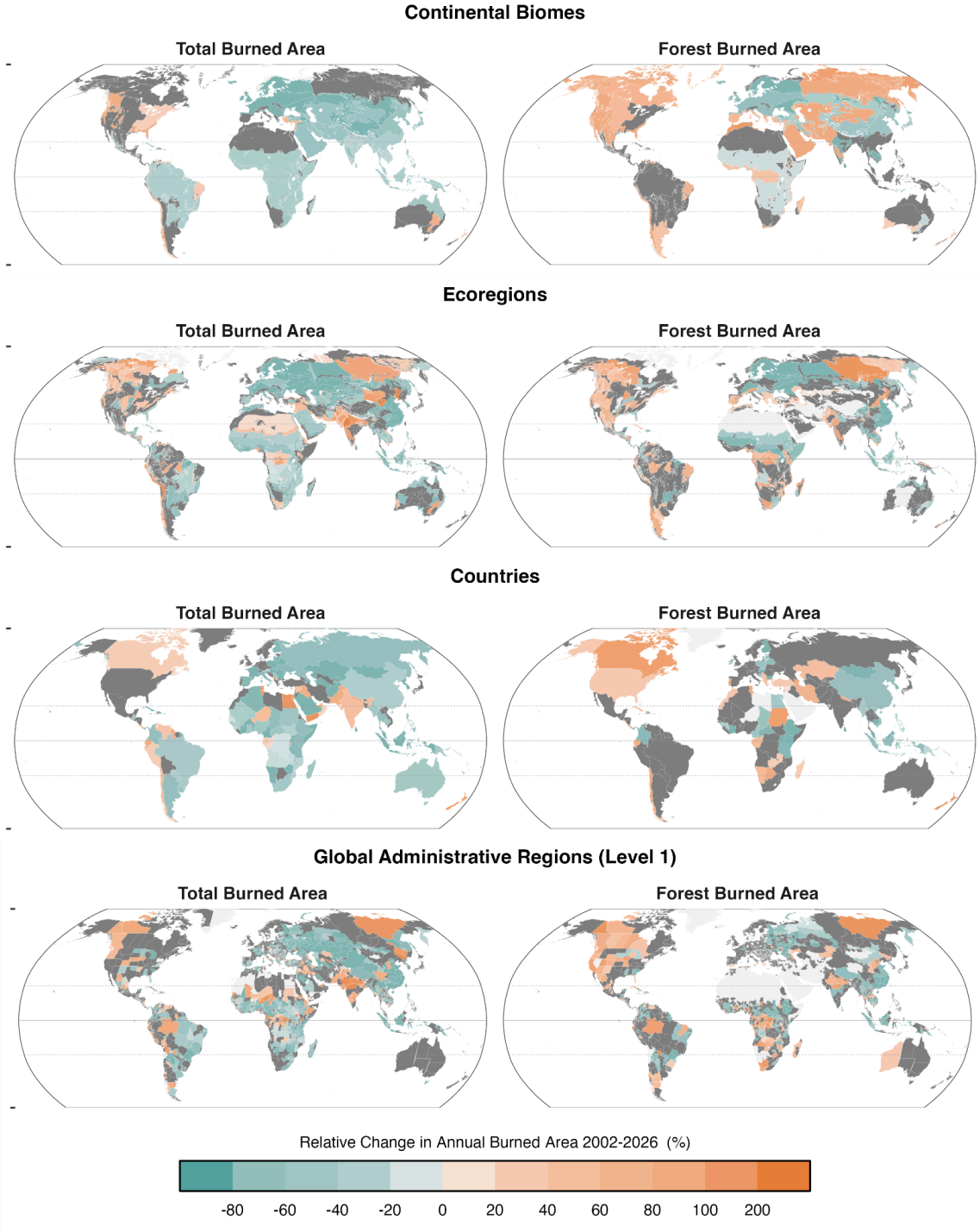


Figure S3: Relative changes (%) in **(left panels)** total annual BA and **(right panels)** forest BA across March-February fire seasons during 2002-2025 for three regional layers: **(top panels)** continental biomes; **(middle panels)** countries, and **(bottom panels)** level 1 administrative regions (e.g., states or provinces). Forest BA considers only areas with tree cover over 30% at the native (500 m) resolution of the BA observations. Relative changes are calculated as the trend in BA across fire seasons March 2002-February 2003 through March 2025-February 2026 multiplied by the number of years in the time series and divided by the mean annual BA during the period. Trends in BA are derived using the Theil-Sen slope estimator. Only significant trends ($p < 0.05$) in BA are shown (dark grey fill signifies no significant trend).

S2.4. Supplementary Analysis: Drought Conditions and Carbon Project Exposure

Drier-than-average conditions were observed across many project regions in 2025, with negative SPEI anomalies recorded in most regions. Over all projects, the SPEI anomaly was 0.52 lower than the 1980-2024 average. Considering that the 2025 fire impact on forest carbon projects was below average even as drought conditions worsened, drought alone could not explain fire exposure. Other factors, such as fuel availability, ignition sources, land-use change, and management practices (e.g. fire-suppression) are crucial in understanding project exposure to fire.

S2.5. Extended Supplementary Figures

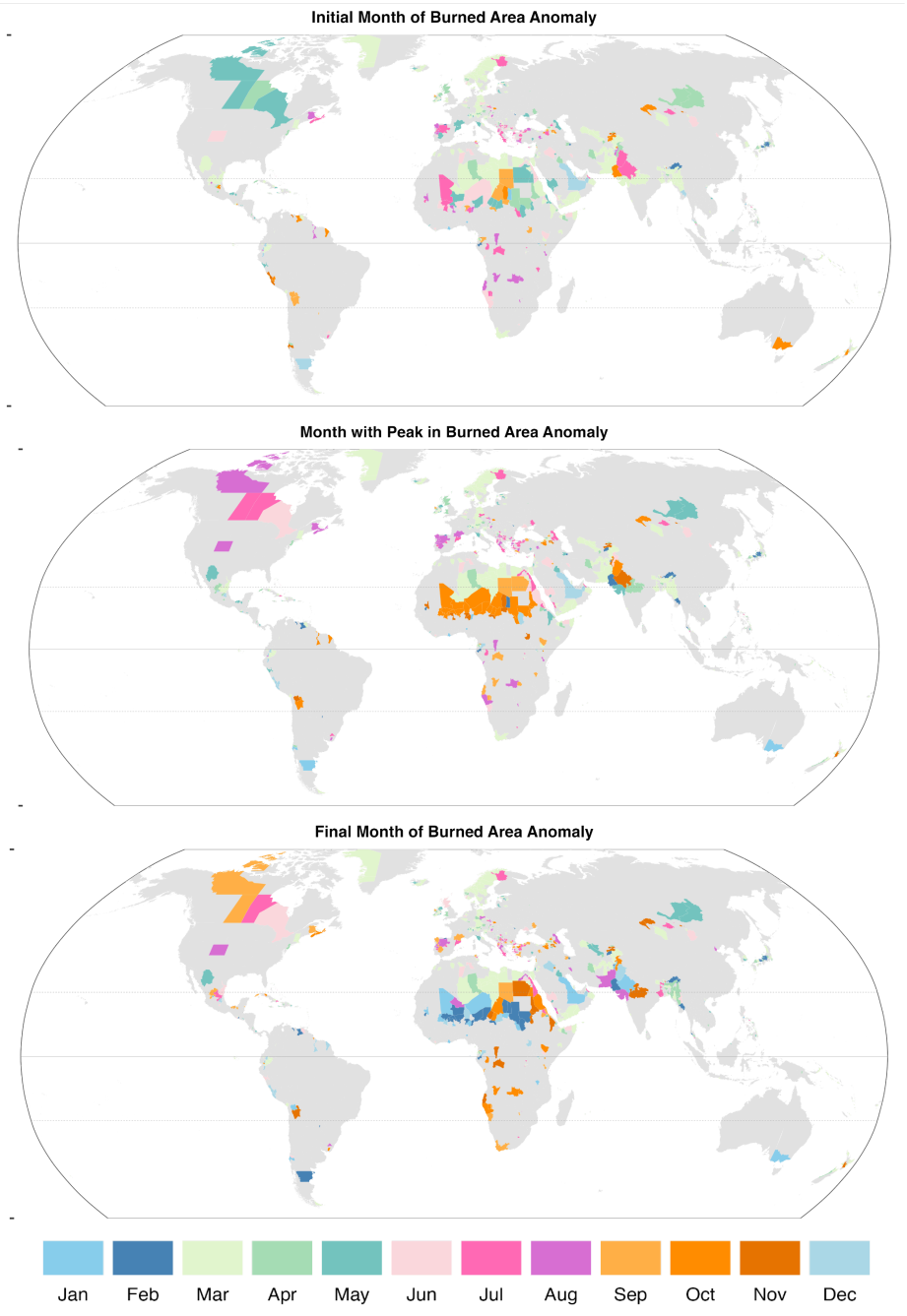


Figure S4: (Top panel) first month, **(middle panel)** peak month, and **(lower panel)** final month of positive BA anomalies at Global Administrative Level 1 during March 2025-February 2026. Peak anomalies are identified relative to the monthly climatology in 2001-2025. The first and final months of the BA anomaly incorporate the period when BA was continuously above the climatological mean. Graduated colours are separated seasonally.

S3. Focal Region 1: Midwestern Canadian Shield Forests

S3.1 Influence of Climate Change

S3.1.1 Changes in Fire Weather

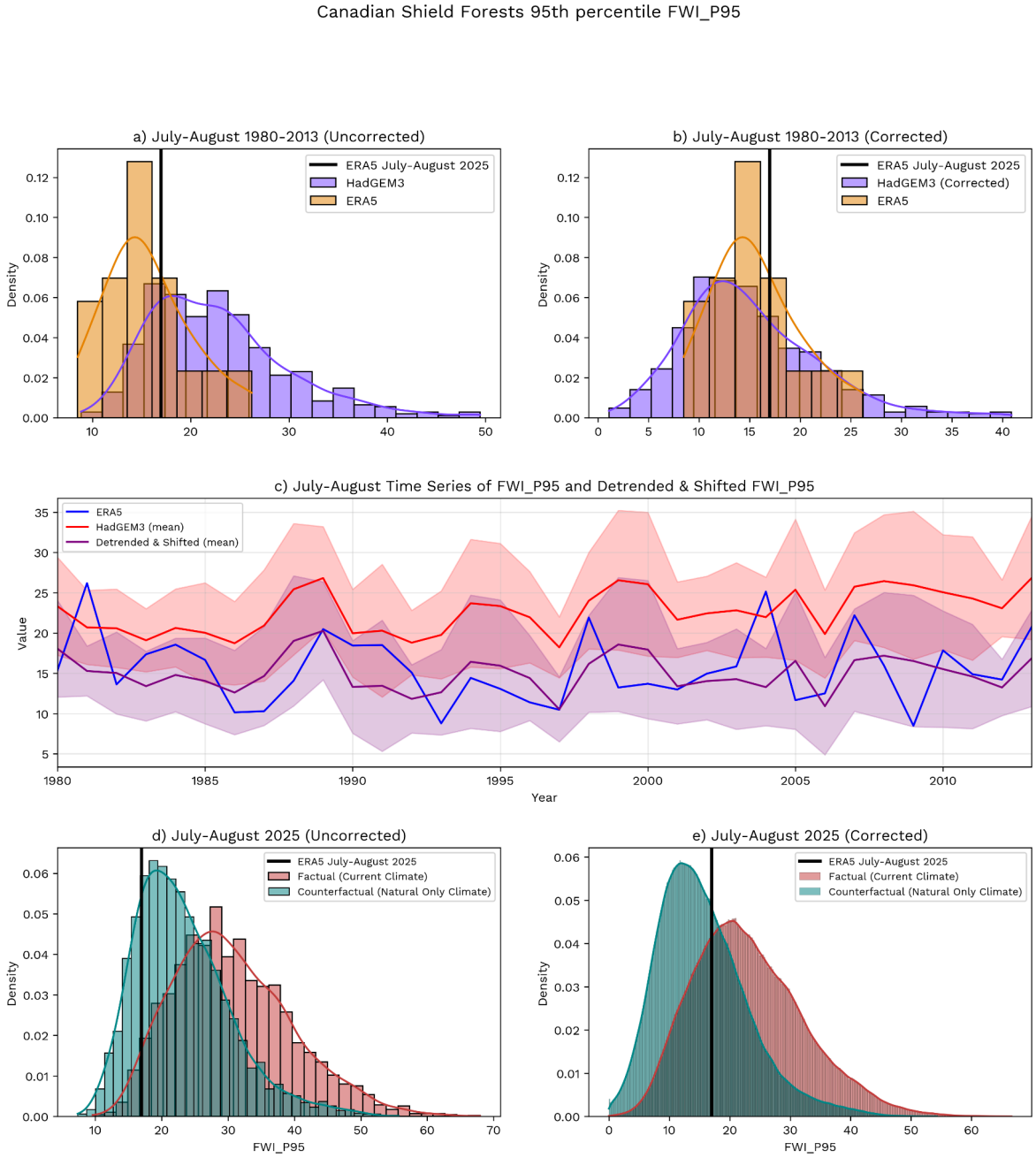


Figure S5: HadGEM3-A Bias Correction. (a): Histogram of uncorrected reanalysis (ERA5) and historical ensemble (HadGEM3-A) results for FWI 95th percentile values for months July-August during the period 1980-2013. Black line denotes the reanalysis value for the FWI 95th percentile value during the event period: July-August 2025 (**FWI = 17.0**). **(b)**: Histogram of corrected model and reanalysis results for FWI 95th percentile values for period July-August 1980-2013. **(c)**: Time-series of uncorrected (red), corrected (purple) model and reanalysis (blue) July-August FWI 95th percentile values for period 1980-2013. Solid Red and Purple lines denote 15 member mean, shading denotes 1std. **(d)**: Uncorrected 525 member attribution ensemble histogram for FWI 95th percentile for 2020-2024, teal representing natural only climate (Counterfactual), red denoting anthropogenically altered climate (Factual). **(e)**: Bias corrected 7875 (525 * 15) member attribution ensemble histogram for 2020-2024, colours assignment unchanged.

Figure S5 details the bias correction applied to the Factual and Counterfactual ensembles as summarised in **S1.2.1**. The uncorrected historical ensemble tends to overestimate the FWI with respect to the reanalysis FWI for the same period (panels a and c). The adjustment corrects for the trend and absolute value (panels b and c). We then apply this bias correction to the present day ensemble to calculate the PR (panel e). With respect to the reanalysis baseline period of 1980-2013, the FWI95 seen during the event in July-August 2025 was slightly above average. During the baseline period the mean FWI95 from ERA5 was 15.7 versus the event value of 17.0. This represents a 8% percent increase over climatology.

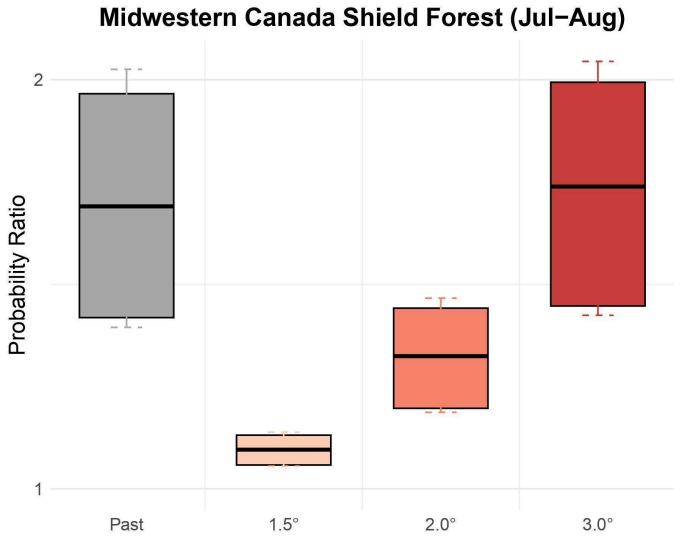


Figure S6: Probability Ratio (PR) estimates based on the comparison between (a) the past climate of 1850-1859 and the recent climate of 2017-2026, the recent climate of 2017–2026 and the period that global mean surface temperature (GMST) reached 1.5 °C, 2 °C and 3 °C for Midwestern Canadian Shieldforests using FWI7X. Results are synthesised based on CanESM5, ACCESS-ESM1-5, and MPI-ESM1-2-LR from CMIP6 models with large (>10) climate ensembles. A 1000-sample non-parametric bootstrapping method is used to give uncertainty estimates for the FWI7X PRs. Bars show 5-95th confidence intervals (CIs), whiskers show 2.5th and 97.5th percentiles, and central values are shown by bold horizontal lines.

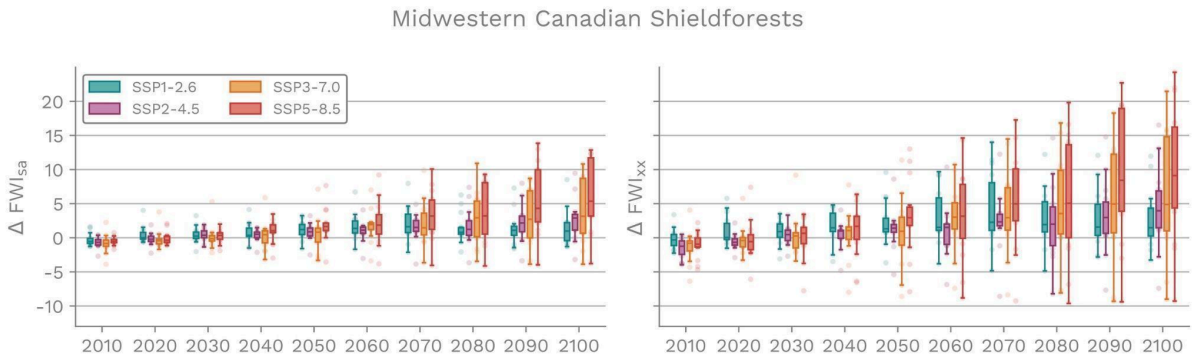


Figure S7: Projected changes in seasonal mean (FWI_{sa}; left) and annual maxima (FWI_{xx}; right) Fire Weather Index (FWI) for the Midwestern Canadian Shield Forests under CMIP6 SSP scenarios, with respect to the reference period 2010-2020. Boxplots show the distribution across CMIP6 models for each decade, with coloured points indicating individual CMIP6 model results, while boxes represent the interquartile range (25th–75th percentiles).

S3.1.2 Changes in Burned Area

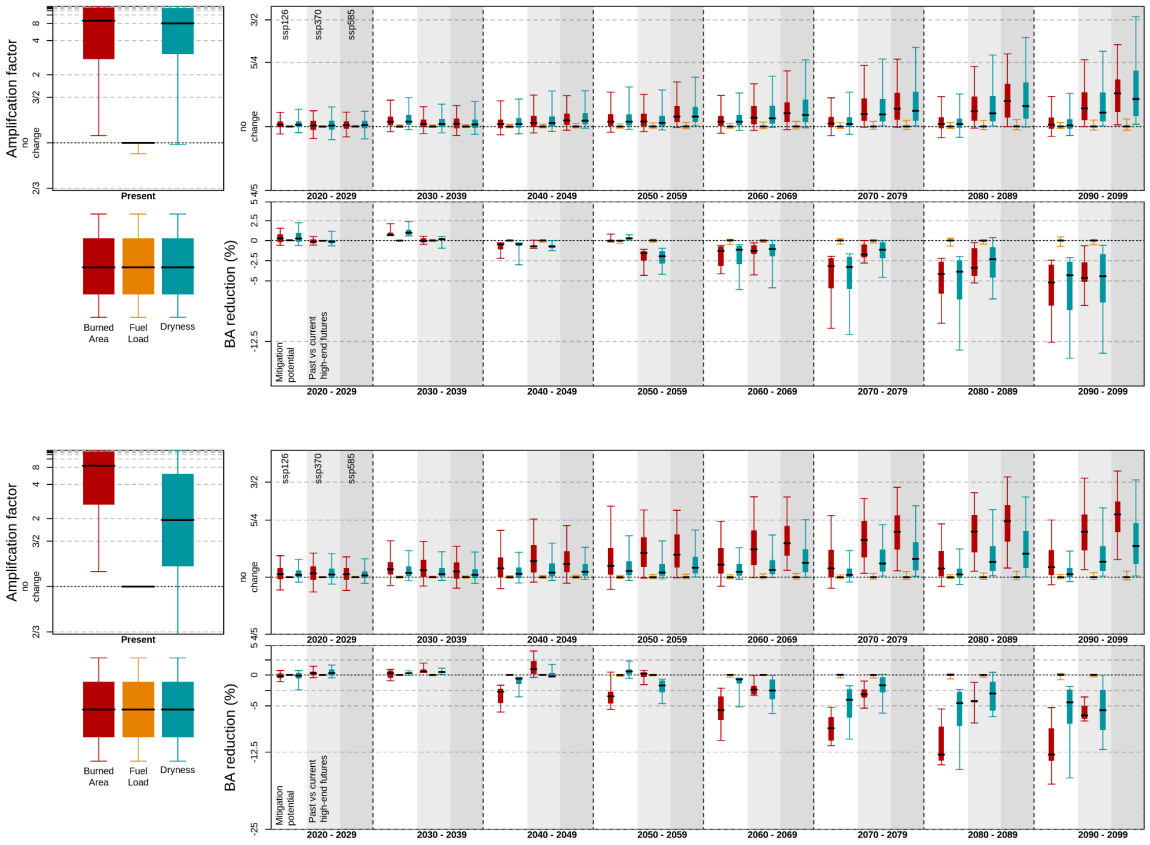


Figure S8: Top two panels per Figure 10 with future projections shown for each decade. Bottom two panels show attribution and projections for sub-regional extremes, i.e for grid cells with top 5% burned area.

Table S7: Focal event burned area attribution and projection results for present day and Shared Socioeconomic Pathway (SSP) scenarios. Colours denote likelihood based on IPCC definitions. Best estimate shown in bold, with 5-95th percentiles in brackets. Mitigation shows the % differences between SSP5-8.5 and SSP3-7.0 AF (in SSP3-7.0 columns) and SSP3-7.0 and SSP1-2.6 (in SSP1-2.6 columns), expressed as 100x (1-lower/high emissions BA)

Table S7: Focal event burned area attribution and projection results for present day and Shared Socioeconomic Pathway (SSP) scenarios. Colours denote likelihood based on IPCC definitions. Best estimate shown in bold, with 5-95th percentiles in brackets. Mitigation shows the % differences between SSP5-8.5 and SSP3-7.0 AF (in SSP3-7.0 columns) and SSP3-7.0 and SSP1-2.6 (in SSP1-2.6 columns), expressed as 100x (1-lower/high emissions BA)

		Present	SSP1-2.6			SSP3-7.0			SSP5-8.5		
			2030s	2040s	2090s	2030s	2040s	2090s	2030s	2040s	2090s
BA	*Probability Ratio*	10.64 (0.97- >100)	1 (0.98,1.04)	1 (0.98, 1.05)	1 (0.98, 1.06)	1 (0.98, 1.04)	1 (0.98,1.07)	1.02 (0.99,1.18)	1 (0.98,1.04)	1.01 (0.99,1.06)	1.05 (0.99,1.28)
	Likelihood	87	68	63	64	61	66	86	59	72	91
	Amplification factor	8.68 (1.04, >100)	1.01 0.99,1.09)	1.01 (0.97, 1.09)	1.01 (0.97, 1.09)	1.01 (0.98, 1.06)	1.01 (0.98, 1.1)	1.06 (1, 1.25)	1.01 (0.97, 1.08)	1.02 (0.99, 1.1)	1.11 (1.01,1.37)
	Likelihood	97	82	67	60	69	73	95	67	84	97
	Mitigation		0.74 (3.21,0.54)	-0.49 (-0.26,-2.11)	-5.16 (-2.54,-12.39)	-0.05 (0.38,-0.05)	-0.56 (0, -0.92)	-4.66 (-0.68,-8.7)			
	Likelihood		0	99	100	54	91	100			
Fuel	*Amplification factor*	1 (0.85, 1)	1 (1, 1)	1 (1, 1.01)	1 (0.99, 1.01)	1 (1, 1.01)	1 (1, 1.01)	1 (0.99, 1.02)	1 (1, 1.01)	1 (1, 1.01)	1 (0.99,1.02)
	Likelihood	45	50	54	57	56	57	57	57	57	57
	Mitigation		-0.02 (0,-0.08)	-0.01 (0, -0.01)	-0.01 (-0.91,0.41)	-0.01 -0.13,0.02)	0 (-0.21,0.08)	0 (-0.38,0.24)			
	Likelihood		99	94	57	85	58	53			
Dryness	*Amplification factor*	7.97 (0.79, >100)	1.01 (0.99, 1.09)	1.01 (0.98, 1.09)	1 (0.97, 1.11)	1.01 (0.98,1.07)	1.01 (0.99,1.12)	1.05 (1, 1.3)	1.01 (0.98, 1.1)	1.02 (0.99, 1.12)	1.1 (1.01, 1.45)
	Likelihood	93	85	69	56	71	77	97	66	87	98
	Mitigation		0.96 (2.07,0.65)	-0.25 (-0.07,-0.25)	-4.55 (-14.75, -2.33)	-0.04 (-2.76,0.38)	-0.69 (-1.49,-0.4)	-4.24 (-10.3, -0.58)			
	Likelihood		0	100	100	52	97	100			

Virtually Certain	Very Likely	Likely	About as likely as not	Unlikely	Very Unlikely	Extremely Unlikely
>99%	>90%	>66%	33-66%	<33%	<10%	<1%

Table S8: Sub-regional burned area extremes attribution and projection results. Sub-regional extremes defined as the grid cells with top 5% BA. Otherwise as per Table S7

		Present	SSP1-2.6			SSP3-7.0			SSP5-8.5		
			2030s	2040s	2090s	2030s	2040s	2090s	2030s	2040s	2090s
BA	*PR*	36.96 (0.48, >100)	1.01 (0.96, 1.09)	1.01 (0.96,1.08)	1.02 0.98,1.16)	1.01 0.97,1.09)	1.03 (0.98,1.17)	1.1 (1, 1.63)	1.01 (0.97, 1.11)	1.03 (0.98,1.15)	1.28 (1.02, 1.7)
	Likelihood	92	73	70	77	72	83	99	72	84	100
	AF	10.55 (1.18, >100)	1.03 (0.96, 1.13)	1.03 (0.96, 1.18)	1.03 0.97,1.26)	1.02 (0.96,1.12)	1.06 (0.97,1.26)	1.23 (1.04,1.52)	1.02 (0.96,1.13)	1.06 (0.98,1.25)	1.27 (1.05,1.58)
	Likelihood	97	79	77	80	71	86	99	71	89	100
	Mitigation		0.9 (1.52, -0.02)	-2.46 (-1.22, -6.59)	-15.73 (-6.67, -17.12)	-0.07 (0.15, -0.07)	-0.25 (0, -1.67)	-3.03 (-1.94, -3.78)			
	Likelihood		5	100	100	56	55	100			
Fuel	*AF*	1 (1, 1)	1 (1, 1)	1 (1, 1.01)	1 (0.99,1.01)	1 (1, 1)	1 (1, 1.01)	1 (0.99,1.02)	1 (1, 1)	1 (1, 1.01)	1 (0.99,1.02)
	Likelihood	45	58	56	54	59	57	54	58	58	55
	Mitigation		0 (0.01, -0.04)	0 (0.02, 0)	0 (-0.79, 0.23)	0 (-0.08, 0.03)	0 (-0.14, 0.04)	-0.01 (-0.35, 0.14)			
	Likelihood		80	84	51	55	65	61			
Dryness	*AF*	1.94 (0.64 >100)	1.02 (0.99, 1.11)	1.01 (0.98, 1.1)	1.01 (0.98, 1.1)	1.01 (0.98, 1.09)	1.01 (0.99, 1.1)	1.06 (1, 1.32)	1.01 (0.98, 1.08)	1.02 (0.99, 1.13)	1.12 (1, 1.48)
	Likelihood	87	81	73	65	75	82	98	63	87	97
	Mitigation		0.8 (2.29, 0.18)	-0.13 (0.27, -0.13)	-4.93 (-2.14, -16.73)	0.42 (0.35, 0.75)	-0.75 (-0.16, -2.35)	-5.37 (-0.01, -10.07)			
	Likelihood		0	69	100	1	99	95			

S3.1.3 Changes in Typical Fire Behaviour

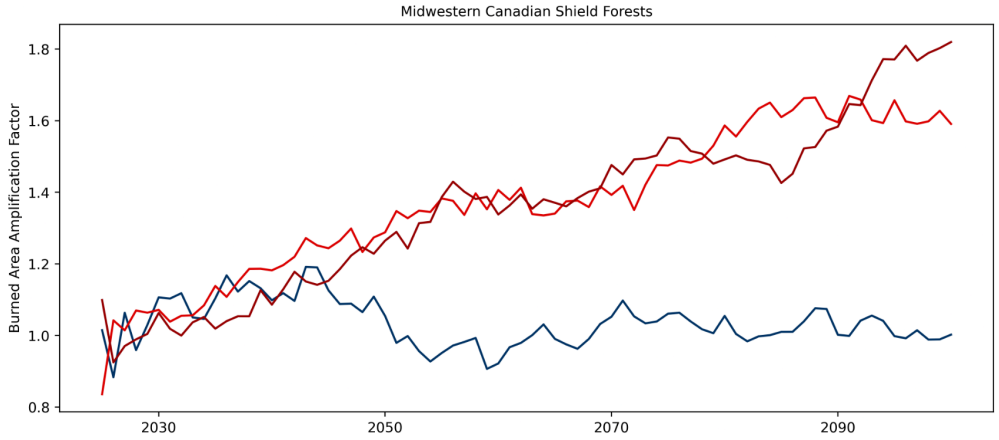


Figure S9: Future projections of burned area (BA) amplification factors (AF) from BuRNN for the 2025-2100 period, considering several Shared Socioeconomic Pathway (SSP) scenarios: SSP1-2.6 (blue), SSP3-7.0 (orange) and SSP5-8.5 (red).

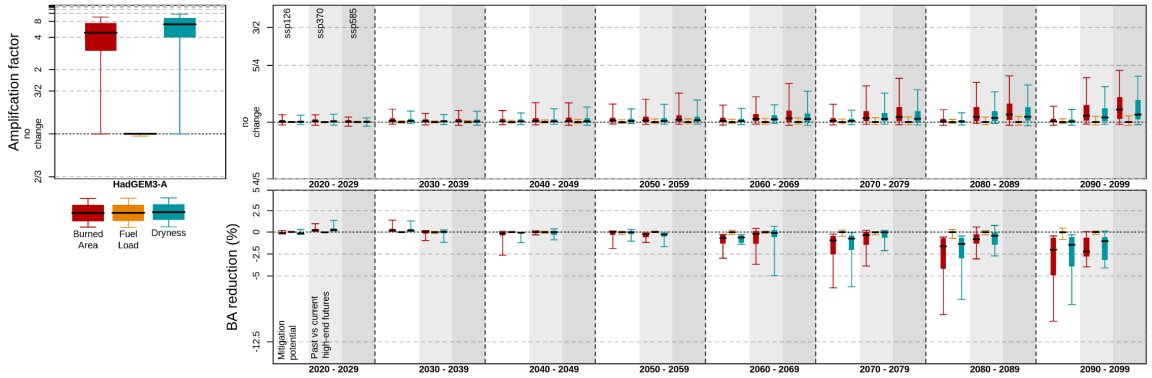


Figure S10: Same as Figure 10 for decade average burned area.

Table S9: Annual average burned area attribution and projection results. Otherwise, as per Table S7

		Present	SSP1-2.6			SSP3-7.0			SSP5-8.5		
			2030s	2040s	2090s	2030s	2040s	2090s	2030s	2040s	2090s
BA	*BURRN*		1.13	1.11	0.99	1.19	1.27	1.63	1.13	1.23	1.8
	PR	5.94 (0.87, 32.73)	1 (1, 1.01)	1 (1, 1.01)	1 (1, 1.03)	1 (1, 1.01)	1.01 (1, 1.02)	1.0 (1.02, 1.14)	1 (1, 1.01)	1 (1, 1.02)	1.04 (1.04, 1.18)
	Likelihood	94	100	80	100	100	100	100	80	100	100
	AF	4.7 (1, 10.91)	1.01 (0.99, 1.05)	1 (0.99, 1.04)	1 (0.99, 1.08)	1 (0.99, 1.03)	1.01 (0.99, 1.08)	1.03 (0.99, 1.2)	1 (0.99, 1.04)	1 (0.99, 1.08)	1.04 (0.99, 1.27)
	Likelihood	97	79	67	66	74	72	85	69	67	89
	Mitigation		0.19 (1.2, 0.11)	-0.2 (-0.08, -3.22)	-2.19 (-0.42, -9.51)	0.06 (0.23, 0.06)	0.04 (0, -0.12)	-1.69 (0.1, -5.45)			
	Likelihood		0	100	100	31	38	93			
Fuel	*AF*	1 (0.98, 1)	1 (1, 1)	1 (1, 1.01)	1 (0.99, 1.01)	1 (1, 1)	1 (1, 1.01)	1 (0.99, 1.02)	1 (1, 1.01)	1 (1, 1.01)	1 (0.99, 1.02)
	Likelihood	36	51	56	57	56	57	58	57	58	58
	Mitigation		-0.02 (0, -0.05)	0 (0.03, 0)	-0.01 (-0.76, 0.3)	0 (-0.17, 0.03)	0 (-0.23, 0.06)	0 (-0.42, 0.23)			
	Likelihood		96	66	61	61	64	61			
Dryness	*AF*	6.76 (1, 14.53)	1 (1, 1.04)	1 (0.99, 1.04)	1 (0.99, 1.06)	1 (0.99, 1.03)	1 (0.99, 1.05)	1.02 (0.99, 1.14)	1 (0.99, 1.04)	1 (0.99, 1.06)	1.03 (0.99, 1.18)
	Likelihood	96	76	66	60	71	72	83	63	66	87
	Mitigation		0.22 (1.17, 0.08)	-0.12 (-0.05, -0.12)	-1.55 (-7.16, -0.3)	0.05 (-0.98, 0.35)	-0.01 (-1, 0.51)	-1.13 (-3.6, 0.11)			
	Likelihood		0	100	100	19	52	94			

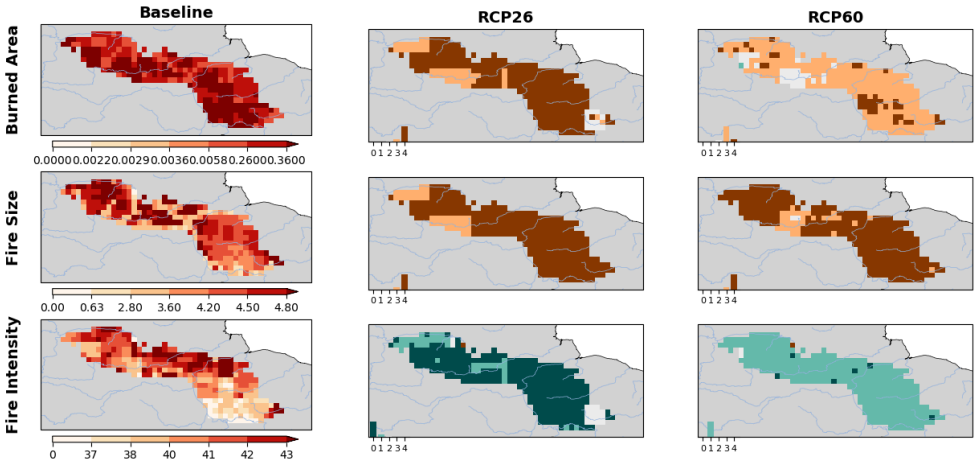


Figure S11: Projected changes in fire characteristics across ISMIP2b GMC future projections taken from Haas et al. (2026). The left column shows modelled baseline conditions for the 2010s, while the right columns show model agreement on the direction of change by 2100 under RCP2.6 (middle) and RCP6.0 (right). Colours indicate the number of models projecting an increase or decrease at each location (brown representing projected increases and blue representing projected decreases). The accompanying histograms (inset) summarise the spatial extent of agreement by showing the fraction of the region where a given number of models agree on the direction of change. Rows correspond (top to bottom) to burned area, fire size, and fire intensity.

S4. Focal Region 2: Northwest Iberia

S4.1. Influence of Climate Change

S4.1.1. Changes in Fire Weather

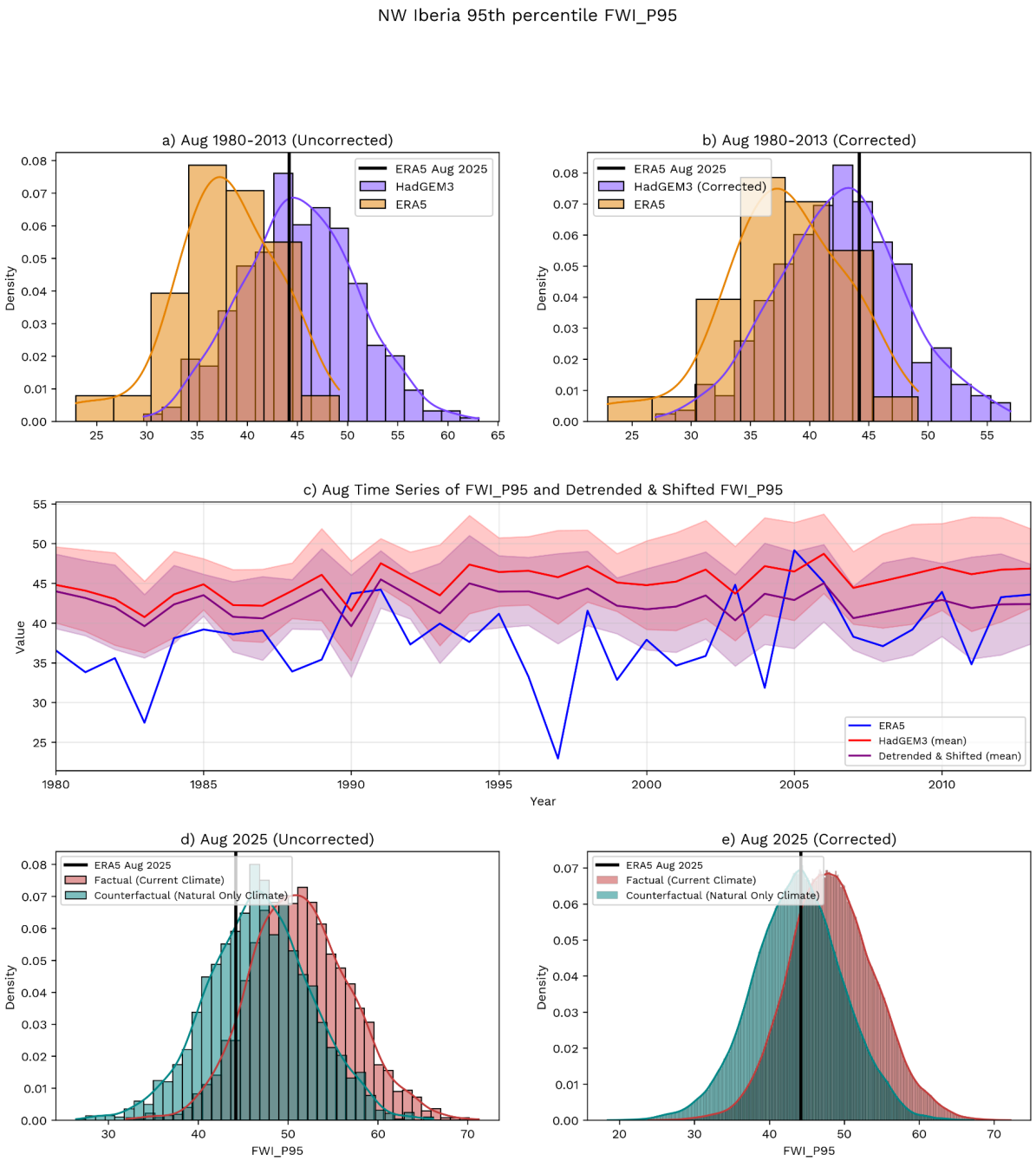


Figure S12: HadGEM3-A Bias Correction. (a): Histogram of uncorrected reanalysis (ERA5) and model (HadGEM3) results for FWI 95th percentile values for August during the period 1980-2013. Black line denotes the ERA5 reanalysis value for the FWI 95th percentile value during the event period: August 2025 (FWI = 44.2). (b): Histogram of corrected model and reanalysis results for FWI 95th percentile values for August 1980-2013. (c): Time-series of uncorrected (red), corrected (purple) model and reanalysis (blue) August FWI 95th percentile values for period 1980-2013. Solid Red and Purple lines

denote 15 member mean, shading denotes 1std. (d) Uncorrected 525 member attribution ensemble histogram for FWI 95th percentile for 2020-2024, teal representing natural only climate, red denoting anthropogenically altered climate. (e) Bias corrected 7875 (525 * 15) member attribution ensemble histogram for 2020-2024, colours assignment unchanged.

Figure S5.1 details the bias correction applied to the two attribution ensembles as summarised in S2.5.1. For this region too, the uncorrected historical ensemble tends to overestimate the FWI with respect to the reanalysis FWI for the same period (panels a and c). The model also underestimates variability in this region, however our bias adjustment only corrects for trend and absolute value (panel c). Therefore the effects of the bias correction were less pronounced here than in the other focal regions. While the bias correction improves the agreement of the distributions, there is a noticeable offset in the reanalysis and historical ensemble distributions (panel b). During the baseline period the mean FWI95 from ERA5 was 39.2. The FWI95 seen during the event in August 2025 was 44.2, representing a 13% increase over climatology.

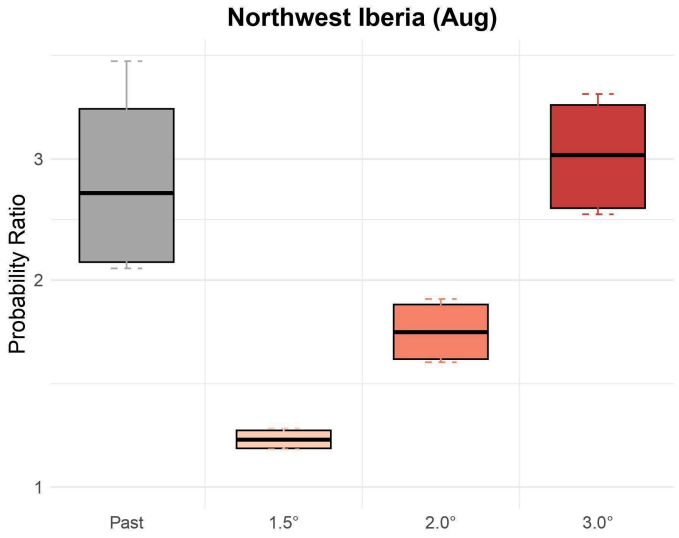


Figure S13: Probability Ratio (PR) estimates based on the comparison between (a) the past climate of 1850-1859 and the recent climate of 2017-2026, the recent climate of 2017–2026 and the period that global mean surface temperature (GMST) reached 1.5 °C, 2 °C and 3 °C for Northwest Iberia using FWI7X. Results are synthesised based on CanESM5, ACCESS-ESM1-5, and MPI-ESM1-2-LR from CMIP6 models with large (>10) climate ensembles. A 1000-sample non-parametric bootstrapping method is used to give uncertainty estimates for the FWI7X PRs. Bars show 5-95th confidence intervals (CIs), whiskers show 2.5th and 97.5th percentiles, and central values are shown by bold horizontal lines.

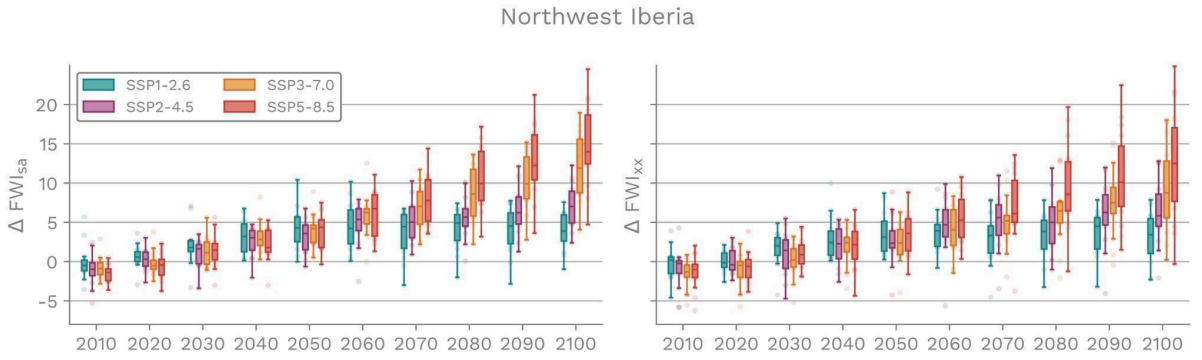


Figure S14: Projected changes in seasonal mean (FWIsa; left) and annual maxima (FWIxx; right) Fire Weather Index (FWI) for Northwest Iberia under CMIP6 SSP scenarios, with respect to the reference period 2010-2020. Boxplots show the distribution across CMIP6 models for each decade, with

coloured points indicating individual CMIP6 model results, while boxes represent the interquartile range (25th–75th percentiles).

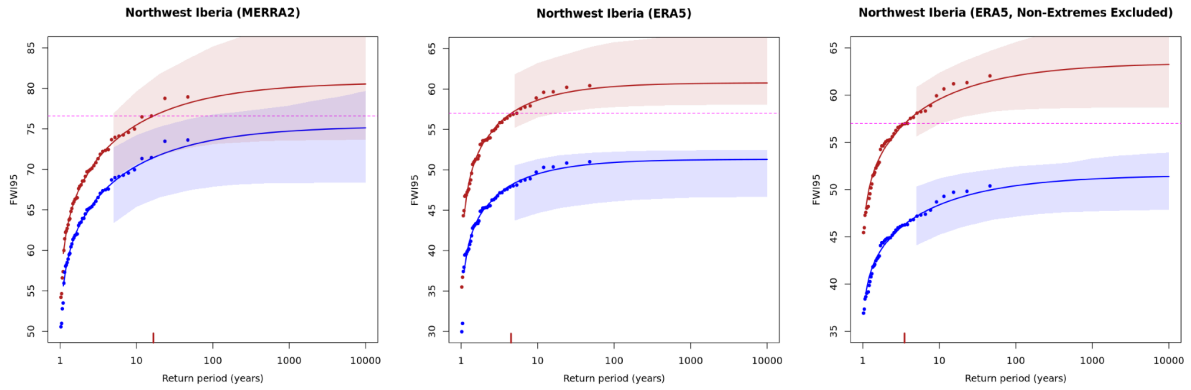


Figure S15: Statistical fits to FWI95. The influence of GMST is shown with the red vs blue probability curves, respectively showing all observed annual maxima as if they had occurred in the present climate (2025-26, red) vs pre-industrial warming levels (blue). The magnitude of the 2025-26 event is highlighted with a horizontal magenta line. Figures are given for the two reanalysis datasets (MERRA2, left, and ERA5, centre), and for ERA5 excluding two low values (right).

Figure S15 shows that across datasets, the PR between preindustrial and present climates is infinite for the central estimate. The CI on the ERA5 return period appears narrow at the upper bound. This is due to the effect of two low values of FWI95 that are not sufficiently close to the tail of the FWI distribution that they are well fit by a GEV distribution, as shown by the CI on the ERA5 return period when those values are excluded. These years were not excluded for the analysis, with that shown here to demonstrate that the infinite return period at all confidence levels is not affected by their inclusion.

S4.1.2. Changes in Burned Area

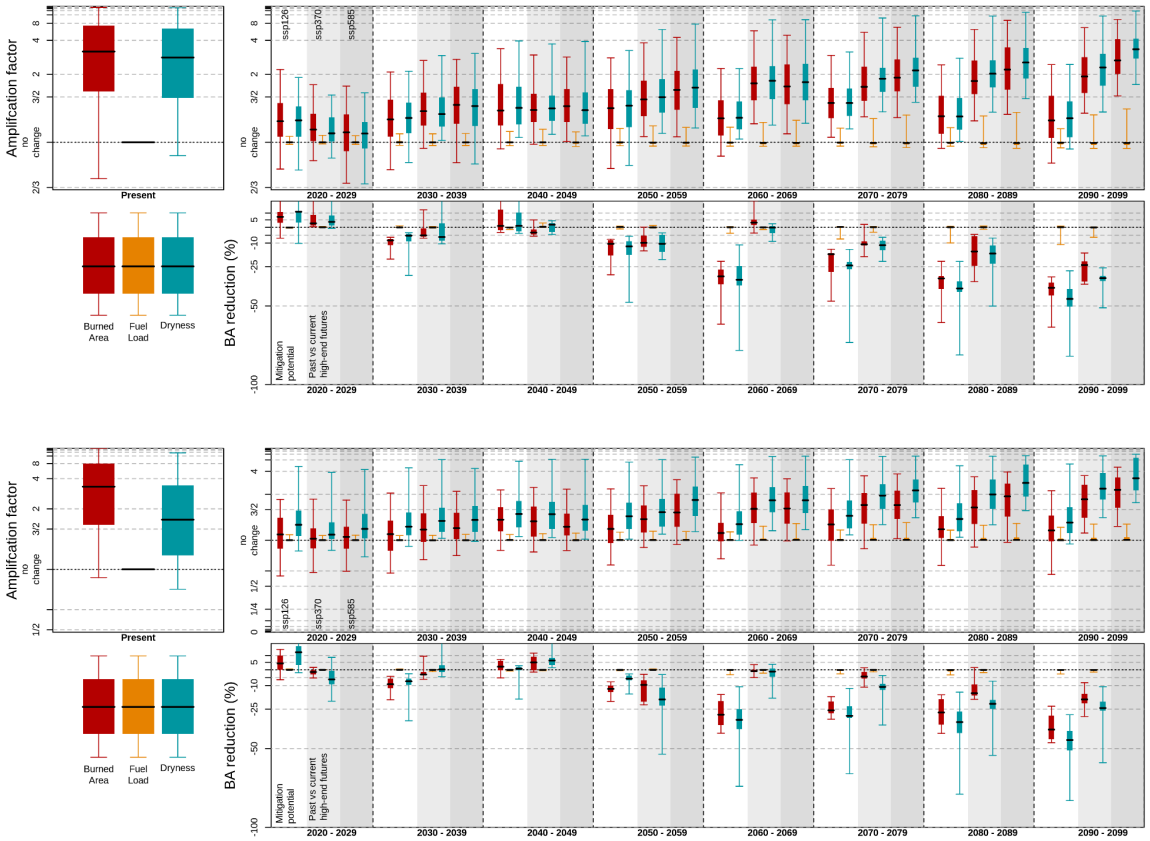


Figure S16: Top two panels per Figure 14 with future projections shown for each decade. Bottom two panels show attribution and projections for sub-regional extremes, i.e for grid cells with top 5% burned area.

Table S10: Focal event burned area attribution and projection results for present day and Shared Socioeconomic Pathway (SSP) scenarios. Colours denote likelihood based on IPCC definitions. Best estimate shown in bold, with 5-95th percentiles in brackets. Mitigation shows the % differences between SSP5-8.5 and SSP3-7.0 AF (in SSP3-7.0 columns) and SSP3-7.0 and SSP1-2.6 (in SSP1-2.6 columns), expressed as 100x (1-lower/high emissions BA).

		Present	SSP1-2.6			SSP3-7.0			SSP5-8.5		
			2030s	*2040s*	*2090s*	*2030s*	*2040s*	*2090s*	*2030s*	*2040s*	*2090s*
BA	*Probability Ratio*	**4.09 (0.51, >100)**	**1.03** (0.93, 1.29)	**1.04** (0.92, 1.37)	**1.01** (0.87, 1.24)	**1.04** (0.94, 1.27)	**1.04** (0.94, 1.33)	**1.08** (0.94, 1.91)	**1.04** (0.93, 1.31)	**1.04** (0.94, 1.26)	**1.09** (0.9, 1.99)
	Likelihood	91	69	70	56	78	77	82	73	75	79
	Amplification factor	**2.93 (0.73, >100)**	**1.18** (0.8, 2.12)	**1.33** (0.96, 2.8)	**1.15** (0.86, 2.15)	**1.27** (0.98, 2.46)	**1.31** (0.98, 2.56)	**1.78** (1.26, 6.84)	**1.32** (0.87, 2.28)	**1.3** (1, 2.28)	**2.33** (1.4, 11.36)
	Likelihood	94	82	93	81	94	94	100	87	95	100
	Mitigation		**-7.96** (-6, -18.68)	**-0.12** (11.38, -2.91)	**-35.55** (-29.34, -68.5)	**-1.99** (12.35, -1.99)	**0.23** (0.24, -1.78)	**-23.35** (-9.95, -34.65)			
	Likelihood		100	45	100	67	46	100			
Fuel	*Amplification factor*	**1** (0.99, 1)	**1** (0.95, 1.08)	**1** (0.94, 1.09)	**1** (0.9, 1.12)	**1** (0.94, 1.07)	**1** (0.94, 1.1)	**0.99** (0.88, 1.27)	**1** (0.94, 1.08)	**1** (0.92, 1.09)	**0.99** (0.9, 1.32)
	Likelihood	48	42	40	32	36	41	33	38	35	34
	Mitigation		**0.04** (1.38, -0.05)	**-0.03** (0.11, -0.03)	**0.32** (-11.57, 1.39)	**0** (-1.33, 0.2)	**0.24** (-0.06, 1.71)	**0.02** (-3, 0.74)			
	Likelihood		15	84	31	59	6	45			
Dryness	*Amplification factor*	**2.64 (0.94, >100)**	**1.23** (0.83, 2.23)	**1.38** (1.04, 3.02)	**1.19** (0.94, 2.15)	**1.28** (1.01, 2.85)	**1.34** (1.07, 4.07)	**2.17** (1.25, 17.43)	**1.37** (0.85, 2.35)	**1.32** (1.03, 2.9)	**3.1** (1.75, 25.89)
	Likelihood	93	85	98	85	96	98	100	86	98	100
	Mitigation		**-6.92** (-2.1, -26.95)	**0.92** (15.72, 0.92)	**-44.93** (-87.64, -26.29)	**-3.75** (-8.1, 22.12)	**2.15** (-3.05, 33.11)	**-30.28** (-47.55, -20.78)			
	Likelihood		100	43	100	69	18	100			

Virtually Certain	Very Likely	Likely	About as likely as not	Unlikely	Very Unlikely	Extremely Unlikely
>99%	>90%	>66%	33-66%	<33%	<10%	<1%

Table S11: Sub-regional burned area extremes attribution and projection results. Sub-regional extremes defined as the grid cells with top 5% BA. Otherwise as per Table S10

		Present	SSP1-2.6			SSP3-7.0			SSP5-8.5		
			2030s	*2040s*	*2090s*	*2030s*	*2040s*	*2090s*	*2030s*	*2040s*	*2090s*
BA	*Probability Ratio*	**5.36 (0.76, >100)**	**0.97** (0.68, 1.1)	**0.96** (0.79, 1.17)	**0.95** (0.73, 1.14)	**0.98** (0.75, 1.15)	**1** (0.81, 1.2)	**1.02** (0.77, 1.39)	**0.98** (0.77, 1.16)	**1.02** (0.83, 1.19)	**1.06** (0.8, 1.46)
	Likelihood	92	37	38	37	43	51	56	42	61	68
	Amplification factor	**3.11 (0.93, >100)**	**1.09** (0.67, 1.98)	**1.28** (0.93, 2.25)	**1.11** (0.67, 1.97)	**1.15** (0.78, 2.15)	**1.2** (0.9, 2.24)	**1.66** (1.07, 3.45)	**1.19** (0.88, 1.99)	**1.17** (0.84, 2.08)	**2.04** (1.2, 4.55)
	Likelihood	94	66	88	68	74	86	97	82	79	99
	Mitigation		**-6.23** (-4.7, -15.75)	**2.58** (7.56, -3.61)	**-33.28** (-25.81, -46.12)	**-3.34** (6.34, -3.34)	**4.79** (0.05, 2.36)	**-19.27** (-12.51, -24.82)			
	Likelihood		100	19	100	86	2	100			
Fuel	*Amplification factor*	**1** (0.94, 1)	**1** (1, 1.09)	**1** (1, 1.1)	**1** (1, 1.15)	**1** (1, 1.07)	**1** (1, 1.11)	**1** (1, 1.19)	**1** (1, 1.09)	**1** (1, 1.09)	**1.01** (1, 1.26)
	Likelihood	48	93	96	87	92	92	90	87	92	96
	Mitigation		**0** (0.9, -0.08)	**0** (0.08, 0)	**-0.1 2** (-4.41, 0)	**0** (-0.99, 0.09)	**0.05** (0, 1.44)	**-0.26** (-4.53, 0)			
	Likelihood		32	46	99	35	18	100			
Dryness	*Amplification factor*	**1.68 (0.87, 45.83)**	**1.22** (0.93, 3.01)	**1.52** (1.05, 4.05)	**1.3** (0.97, 3.07)	**1.28** (0.96, 4.57)	**1.4** (1.02, 4.27)	**2.35** (1.24, 8.76)	**1.3** (0.99, 2.79)	**1.34** (0.98, 4.63)	**3.25** (1.77, 11.58)
	Likelihood	90	90	99	93	93	97	100	91	93	100
	Mitigation		**-4.71** (-2.03, -19.78)	**4.82** (9.55, 4.82)	**-45.06** (-62.07, -22.8)	**0.55** (-3.79, 17.87)	**4.13** (-6.64, 7)	**-29.57** (-42.08, -18.27)			
	Likelihood		100	10	100	43	33	100			

S4.1.3 Changes in Typical Fire Behaviour

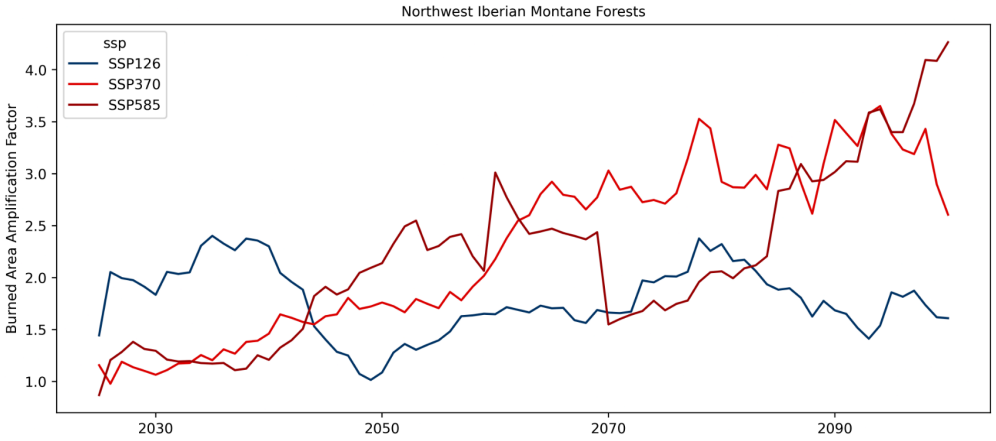


Figure S17: Future projections of burned area (BA) amplification factors (AF) from BuRNN for the 2025-2100 period, considering several Shared Socioeconomic Pathway (SSP) scenarios: SSP1-2.6 (blue), SSP3-7.0 (orange) and SSP5-8.5 (red).

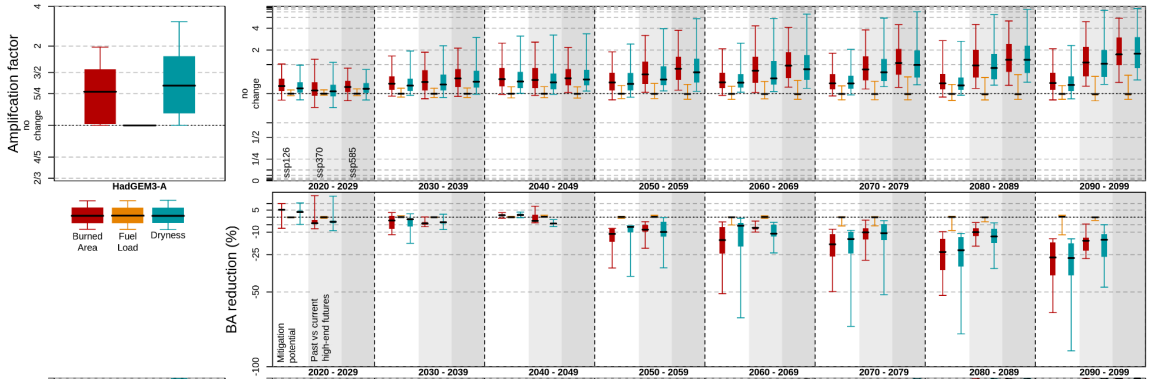


Figure S18: same as **Figure 14**, but for all simulated BAs to calculate amplification for the annual average burned area. Future calculations of amplification factor here use unconditioned BA as described in **Section 1.2.4.**

Table S12: Annual average burned area attribution and projection results. Otherwise, as per Table S10

		Present	SSP1-2.6			SSP3-7.0			SSP5-8.5		
			2030s	*2040s*	*2090s*	*2030s*	*2040s*	*2090s*	*2030s*	*2040s*	*2090s*
BA	***BURNN***		2.36	1.01	1.62	1.38	1.72	2.9	1.25	2.09	4.09
	Probability Ratio	**1.25** (0.83, 12.47)	**3.7** (1.74, 12.61)	**11.31** (3.15, 16.21)	**6.67** (1.94, 8.69)	**8.39** (2.33, 38.84)	**7.47** (2.59, 35.43)	**60.92** (28.36, 94.83)	**3.43** (1.82, 6.62)	**5.96** (4.8, 8.45)	**>100** (47.91, >100)
	Likelihood	83	100	100	100	100	100	100	100	100	100
	Amplification factor	**1.27** (1, 1.97)	**1.15** (0.99, 1.87)	**1.18** (1, 2.45)	**1.14** (0.89, 2.07)	**1.17** (0.97, 2.04)	**1.2** (1, 2.67)	**1.52** (1.09, 5.31)	**1.24** (0.99, 2.07)	**1.22** (1.03, 2.22)	**1.98** (1.16, 7.58)
	Likelihood	94	92	94	83	90	95	99	95	98	100
	Mitigation		**-2.03** (1.15, -12.18)	**-0.89** (0.92, -5.52)	**-25.15** (-15.65, -60.93)	**-4.95** (0.44, -4.95)	**-1.86** (0.17, -3.49)	**-23.15** (-6.3, -37.08)			
	Likelihood		77	68	100	95	71	100			
Fuel	*Amplification factor*	**1** (1, 1)	**1** (0.96, 1.07)	**1** (0.95, 1.08)	**1** (0.93, 1.11)	**1** (0.96, 1.07)	**1** (0.95, 1.09)	**0.99** (0.93, 1.22)	**1** (0.95, 1.06)	**1** (0.95, 1.08)	**1** (0.93, 1.32)
	Likelihood	49	39	39	33	38	41	35	35	35	38
	Mitigation		**0.07** (0.86, 0)	**0** (0.08, 0)	**0.09** (-9.68, 0.58)	**0.13** (0, 0.75)	**0.17** (0, 1.4)	**-0.06** (-10.74, 0.13)			
	Likelihood		11	62	42	6	2	82			
Dryness	*Amplification factor*	**1.33** (1, 2.89)	**1.11** (0.98, 2.07)	**1.15** (1.01, 2.77)	**1.1** (0.93, 2.37)	**1.12** (0.98, 2.21)	**1.14** (1.01, 3.55)	**1.49** (1.11, 13.25)	**1.16** (1, 2.81)	**1.2** (1.04, 2.75)	**1.95** (1.2, 45.07)
	Likelihood	98	91	96	81	92	96	100	95	99	100
	Mitigation		**-0.7** (-0.08, -15.76)	**0.33** (1.4, 0.33)	**-26.42** (-82.17, -15.34)	**-3.5** (-9.49, -1.51)	**-4.01** (-4.86, 21.19)	**-22.78** (-63.74, -7.72)			
	Likelihood		96	36	100	96	83	100			

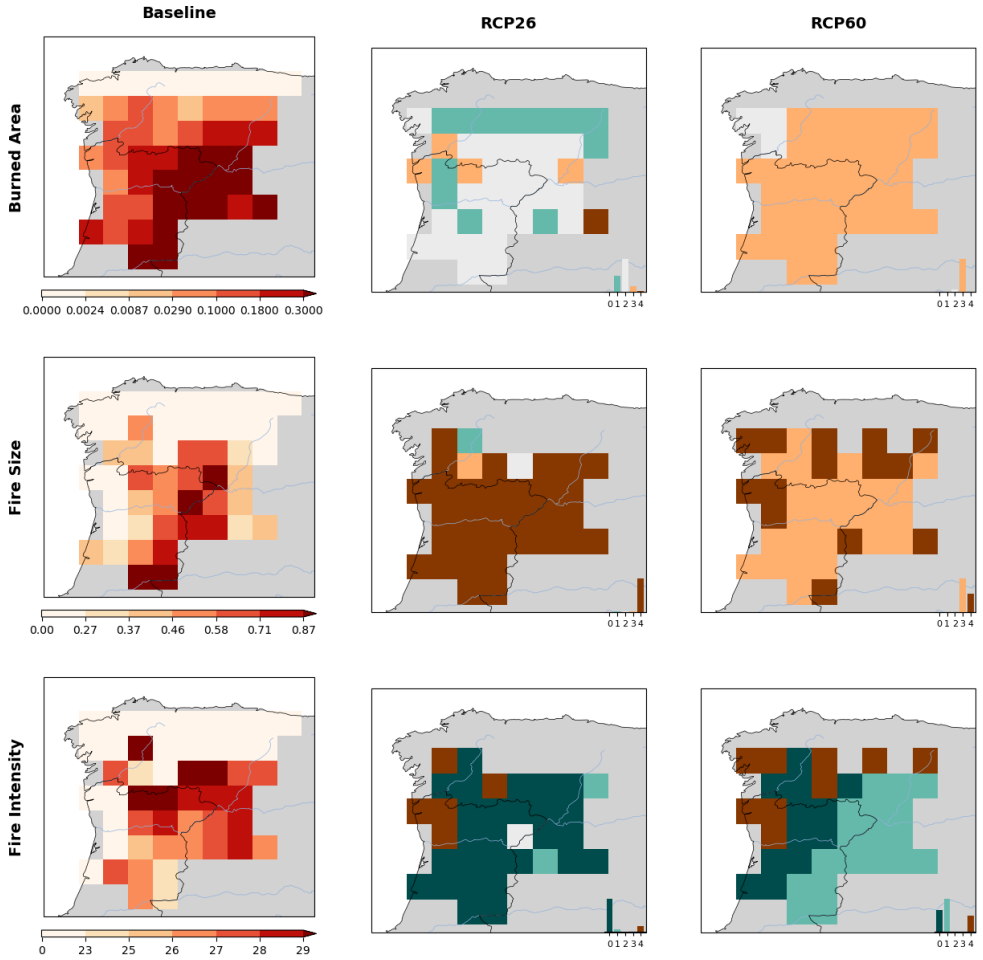


Figure S19. Projected changes in fire characteristics across ISMIP2b GMC future projections taken from Haas et al. (2026). The left column shows modelled baseline conditions for the 2010s, while the right columns show model agreement on the direction of change by 2100 under RCP2.6 (middle) and RCP6.0 (right). Colours indicate the number of models projecting an increase or decrease at each location (brown representing projected increases and blue representing projected decreases). . The accompanying histograms summarise the spatial extent of agreement by showing the fraction of the region where a given number of models agree on the direction of change. Rows correspond (top to bottom) to burned area, fire size, and fire intensity.

S5. Focal Region 3: Chilean Temperate Forests and Matorral

S5.1. Influence of Climate Change

S5.1.1. Changes in Fire Weather

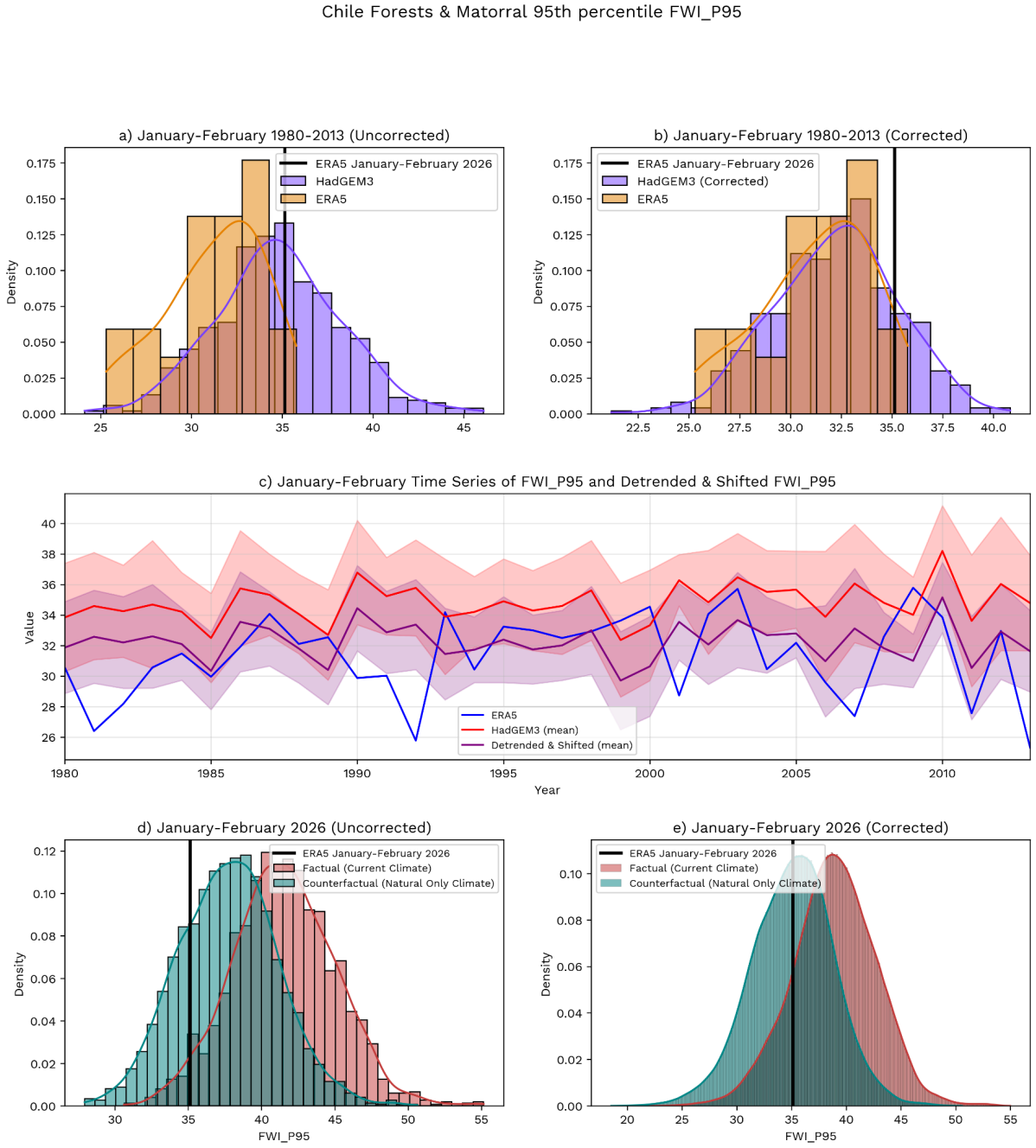


Figure S20: **HadGEM3-A Bias Correction.** (a): Histogram of uncorrected reanalysis (ERA5) and model (HadGEM3) results for FWI 95th percentile values for months July-August during the period 1980-2013. Black line denotes the ERA5 reanalysis value for the FWI 95th percentile value during the event period: **January-February 2026** (**FWI = 35.1**). **(b)**: Histogram of corrected model and reanalysis results for FWI 95th percentile values for period January-February 1980-2013.**(c):** Time-series of uncorrected (red), corrected (purple) model and reanalysis (blue) January-February FWI 95th percentile values for period 1980-2013. Solid Red and Purple lines denote 15 member mean, shading

denotes 1std. **(d):** Uncorrected 525 member attribution ensemble histogram for FWI 95th percentile for 2020-2024, teal representing natural only climate, red denoting anthropogenically altered climate. **(e):** Bias corrected 7875 (525 * 15) member attribution ensemble histogram for 2020-2024, colours assignment unchanged.

Figure S20 details the bias correction applied to the two attribution ensembles as summarised in **S1.2.1.** The uncorrected historical ensemble tends to overestimate the FWI at the higher end of the distribution. Nudges to the FWI95 value from the historical ensemble brought it into good alignment with the reanalysis values and when applied to the attribution ensemble generated sensible values in agreement with model synthesis. With respect to the reanalysis baseline period of 1980-2013, the FWI95 seen during the event in January-February 2026 was above average, and sits in the highest part of the historical distribution (panel a). During the baseline period the mean FWI95 from ERA5 was 32.6versus the event value of 35.1. This represents a 7% increase over the climatology.

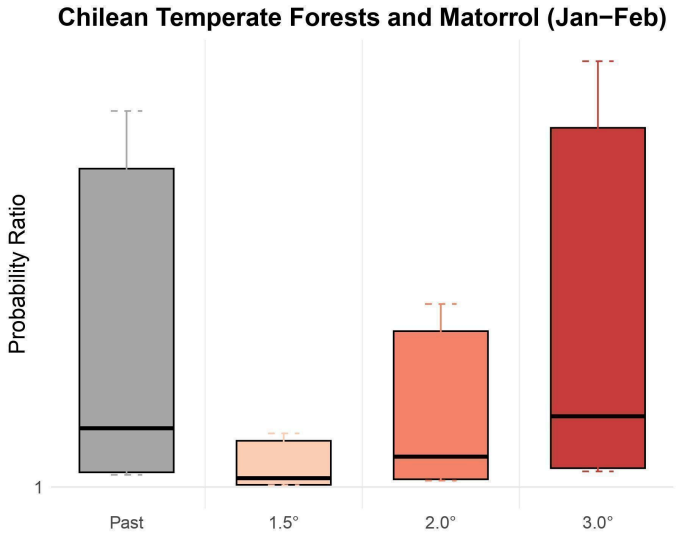


Figure S21: Probability Ratio (PR) estimates based on the comparison between (a) the past climate of 1850-1859 and the recent climate of 2017-2026, the recent climate of 2017–2026 and the period that global mean surface temperature (GMST) reached 1.5 °C, 2 °C and 3 °C for Chilean Temperate Forests and Matorral using FWI7X. Results are synthesised based on CanESM5, ACCESS-ESM1-5, and MPI-ESM1-2-LR from CMIP6 models with large (>10) climate ensembles. A 1000-sample non-parametric bootstrapping method is used to give uncertainty estimates for the FWI7X PRs. Bars show 5-95th confidence intervals (CIs), whiskers show 2.5th and 97.5th percentiles, and central values are shown by bold horizontal lines.

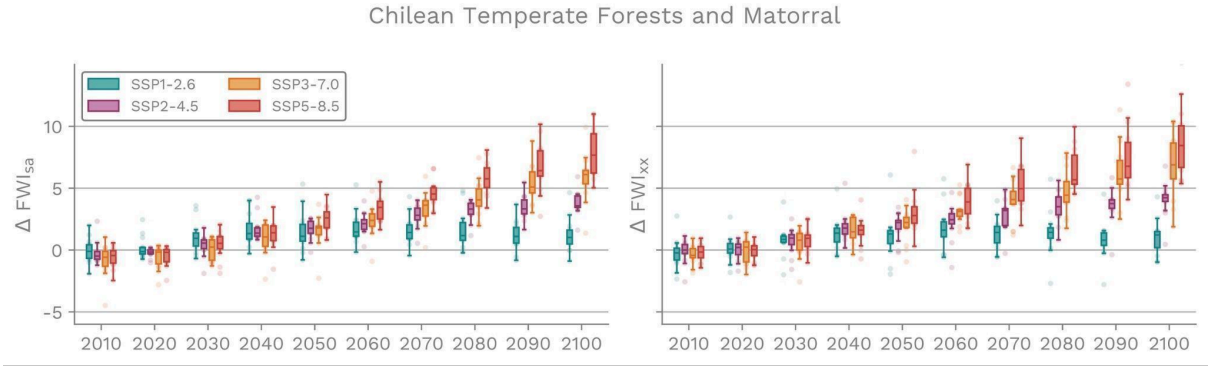


Figure S22: Projected changes in seasonal mean (FWI_{sa}; left) and annual maxima (FWI_{xx}; right) Fire Weather Index (FWI) for the Chilean Temperate Forests and Mattoral under CMIP6 SSP scenarios, with respect the reference period 2010-2020. Boxplots show the distribution across CMIP6 models for each decade, with coloured points indicating individual CMIP6 model results, while boxes represent the interquartile range (25th–75th percentiles).

S5.1.2. Changes in Burned Area

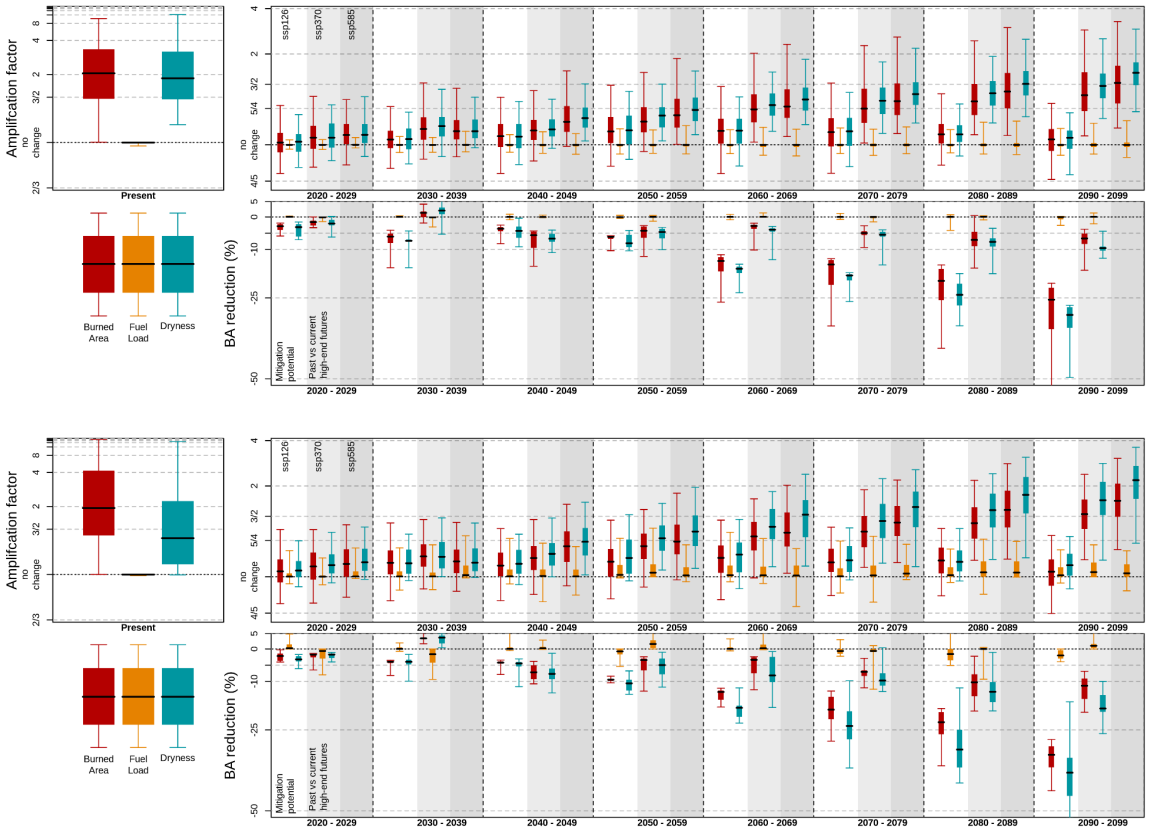


Figure S23: Top two panels per Figure 18 with future projections shown for each decade. Bottom two panels show attribution and projections for sub-regional extremes, i.e for grid cells with top 5% burned area.

Table S13: Focal event burned area attribution and projection results for present day and Shared Socioeconomic Pathway (SSP) scenarios. Colours denote likelihood based on IPCC definitions. Best estimate shown in bold, with 5-95th percentiles in brackets. Mitigation shows the % differences between SSP5-8.5 and SSP3-7.0 AF (in SSP3-7.0 columns) and SSP3-7.0 and SSP1-2.6 (in SSP1-2.6 columns), expressed as 100x(1-lower/high emissions BA).

		Present	SSP1-2.6			SSP3-7.0			SSP5-8.5		
			2030s	*2040s*	*2090s*	*2030s*	*2040s*	*2090s*	*2030s*	*2040s*	*2090s*
BA	*Probability Ratio*	**2.06 (0.83, 26.17)**	**1.02** (0.93, 1.18)	**1.03** (0.93, 1.26)	**1.03** (0.92, 1.25)	**1.04** (0.96, 1.32)	**1.05** (0.96, 1.31)	**1.15** (1, 1.87)	**1.04** (0.96, 1.25)	**1.07** (0.98, 1.39)	**1.19** (1.02, 2.34)
	Likelihood	93	68	75	69	81	82	96	82	90	96
	Amplification factor	**2.04 (1.00, 11.87)**	**1.03** (0.83, 1.28)	**1.04** (0.87, 1.33)	**1.03** (0.8, 1.36)	**1.08** (0.91, 1.48)	**1.07** (0.92, 1.42)	**1.34** (1.05, 2.64)	**1.07** (0.93, 1.45)	**1.13** (0.99, 1.63)	**1.47** (1.07, 3.17)
	Likelihood	95	65	69	66	82	84	97	83	94	98
	Mitigation		**-5.77** (-4.46, -12.64)	**-3.45** (-3.09, -5.61)	**-24.1** (-18.57, -48.54)	**1.33** (2.6, 1.33)	**-5.33** (-0.03, -12.99)	**-9.04** (-2.47, -17.44)			
	Likelihood		100	99	100	24	100	100			
Fuel	*Amplification factor*	**1** (0.89, 1)	**1** (0.97, 1.05)	**1** (0.96, 1.08)	**1** (0.95, 1.09)	**1** (0.96, 1.04)	**1** (0.95, 1.06)	**1** (0.94, 1.14)	**1** (0.97, 1.06)	**1** (0.96, 1.06)	**1** (0.94, 1.16)
	Likelihood	45	35	37	39	34	37	40	40	38	41
	Mitigation		**0.06** (0.91, -0.08)	**0.07** (1.13, 0.07)	**0** (-3.03, 0.59)	**-0.24** (-1.6, -0.01)	**-0.03** (-0.45, 0.03)	**-0.1** (-1.96, 0.05)			
	Likelihood		6	17	48	100	88	71			
Dryness	*Amplification factor*	**1.94 (1.07, 10.42)**	**1.03** (0.87, 1.23)	**1.05** (0.9, 1.28)	**1.05** (0.83, 1.23)	**1.11** (0.91, 1.37)	**1.09** (0.97, 1.32)	**1.47** (1.17, 2.09)	**1.07** (0.96, 1.35)	**1.17** (1.02, 1.48)	**1.66** (1.26, 2.6)
	Likelihood	98	63	71	70	82	89	100	88	96	100
	Mitigation		**-7.26** (-4.64, -11.1)	**-4.21** (-3.22, -4.21)	**-29.27** (-41.92, -26.33)	**2.76** (-4.55, 3.55)	**-6.47** (-8.72, -5.02)	**-10.58** (-19.16, -6.43)			
	Likelihood		100	100	100	27	100	100			

Virtually Certain	Very Likely	Likely	About as likely as not	Unlikely	Very Unlikely	Extremely Unlikely
>99%	>90%	>66%	33-66%	<33%	<10%	<1%

Table S14: Sub-regional burned area extremes attribution and projection results. Sub-regional extremes, defined as the grid cells with the top 5% BA. Otherwise as per Table S13

		Present	SSP1-2.6			SSP3-7.0			SSP5-8.5		
			2030s	*2040s*	*2090s*	*2030s*	*2040s*	*2090s*	*2030s*	*2040s*	*2090s*
BA	*Probability Ratio*	**2.02 (0.91, >100)**	**1.05** (0.91, 1.22)	**1.04** (0.89, 1.22)	**1.03** (0.9, 1.22)	**1.05** (0.93, 1.27)	**1.06** (0.94, 1.25)	**1.18** (1, 1.5)	**1.05** (0.92, 1.26)	**1.08** (0.93, 1.32)	**1.24** (1.03, 1.69)
	Likelihood	93	74	71	69	78	84	95	78	81	97
	Amplification factor	**2.02 (1.01, 96.5)**	**1.08** (0.85, 1.37)	**1.07** (0.88, 1.34)	**1.04** (0.82, 1.29)	**1.13** (0.89, 1.47)	**1.11** (0.9, 1.43)	**1.49** (1.06, 2.29)	**1.09** (0.87, 1.4)	**1.16** (0.94, 1.55)	**1.65** (1.09, 2.76)
	Likelihood	97	75	73	61	82	82	96	79	87	97
	Mitigation		**-3.98** (-3.01, -7.88)	**-3.94** (-1.89, -6.35)	**-30.29** (-22.48, -43.65)	**2.43** (5.33, 2.43)	**-4.17** (0.16, -7.18)	**-9.61** (-3.89, -17.25)			
	Likelihood		100	99	100	0	99	99			
Fuel	*Amplification factor*	**1** (0.98, 1)	**1** (0.93, 1.2)	**1.01** (0.95, 1.26)	**1.01** (0.93, 1.16)	**1** (0.92, 1.15)	**1** (0.83, 1.2)	**1.03** (1, 1.26)	**1.01** (1, 1.27)	**1** (0.87, 1.21)	**1.02** (0.93, 1.2)
	Likelihood	44	71	77	78	71	75	92	84	70	88
	Mitigation		**0.19** (4.27, -0.04)	**0.29** (10.86, 0.29)	**-3.1** (-8.71, -0.04)	**-2.04** (-10.41, -0.01)	**0.16** (-1.79, 1.36)	**0.84** (0.01, 9.16)			
	Likelihood		21	0	100	100	16	0			
Dryness	*Amplification factor*	**1.41 (1.00, 44.2)**	**1.1** (0.98, 1.31)	**1.09** (0.99, 1.38)	**1.07** (0.95, 1.31)	**1.13** (1, 1.5)	**1.16** (1.01, 1.52)	**1.75** (1.13, 2.61)	**1.08** (1, 1.42)	**1.23** (1.02, 1.63)	**2.1** (1.21, 3.27)
	Likelihood	93	88	89	83	94	97	100	94	98	100
	Mitigation		**-2.96** (-1.28, -12.65)	**-5.66** (-2.42, -5.66)	**-39.11** (-49.87, -16.71)	**4.09** (-0.06, 7.7)	**-5.56** (-10.24, -1.37)	**-16.04** (-21.42, -6.74)			
	Likelihood		99	99	100	8	97	100			

S5.1.3 Changes in Typical Fire Behaviour

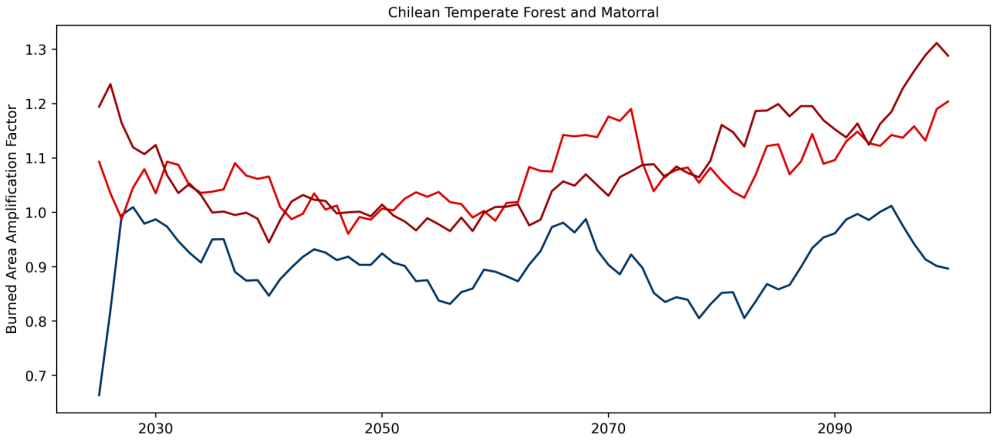


Figure S24: Future projections of burned area (BA) amplification factors (AF) from BuRNN for the 2025-2100 period relative to 2010-2019, considering several Shared Socioeconomic Pathway (SSP) scenarios: SSP1-2.6 (blue), SSP3-7.0 (orange) and SSP5-8.5 (red).

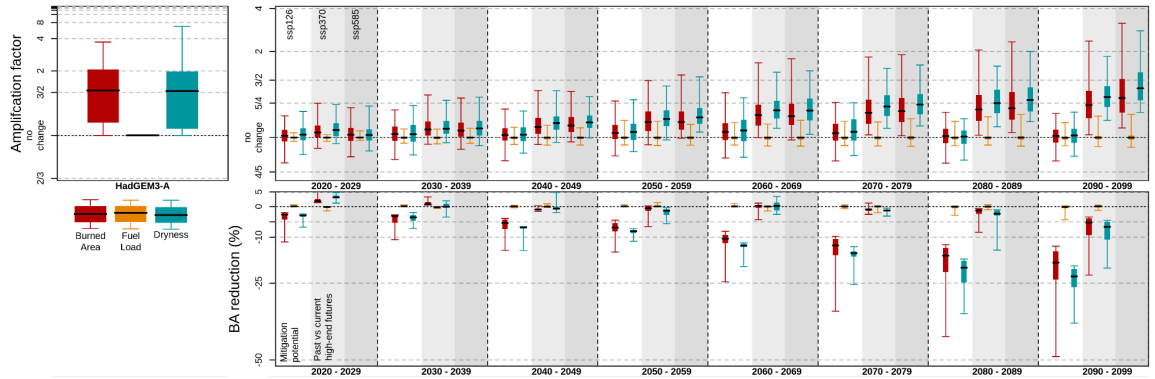


Figure S25: same as **Figure 18**, but for all simulated burned areas (BA) to calculate amplification factors (AF) for the annual average BA using ConFLAME. Future calculations of AF here use unconditioned BA as described in **Section 1.2.4.**

Table S15: Annual average burned area attribution and projection results. Otherwise, as per Table S13

		Present	SSP1-2.6			SSP3-7.0			SSP5-8.5		
			2030s	***2040s***	***2090s***	***2030s***	***2040s***	***2090s***	***2030s***	***2040s***	***2090s***
	BURNN		0.88	0.9	0.9	1.06	0.99	1.19	0.99	0.99	1.31
BA	*Probability Ratio*	**1.48** (0.39, 8.64)	**1.07** (1.01, 1.12)	**1.05** (1.02, 1.23)	**1.04** (1.02, 1.07)	**1.08** (1.06, >100)	**1.21** (1.06, >100)	**2.8** (1.52, >100)	**19.78** (1.16, >100)	**1.09** (1.07, 1.78)	**11.16** (2.3, >100)
	Likelihood	91	100	100	100	100	100	100	100	100	100
	Amplification factor	**1.54** (1, 3.62)	**1.02** (0.9, 1.21)	**1.01** (0.87, 1.17)	**1.01** (0.85, 1.17)	**1.05** (0.97, 1.33)	**1.06** (0.97, 1.35)	**1.23** (1.02, 2.27)	**1.04** (0.95, 1.26)	**1.07** (0.96, 1.39)	**1.29** (1.04, 2.94)
	Likelihood	94	64	62	59	85	85	97	79	88	97
	Mitigation		**-3.26** (-2.95, -10.31)	**-5.38** (-3.81, -14.94)	**-18.3** (-13.29, -48.51)	**1.21** (5.37, 1.21)	**-0.84** (-0.02, -2.18)	**-4.96** (-1.84, -22.35)			
	Likelihood		100	100	100	1	94	98			
Fuel	*Amplification factor*	**1** (1, 1)	**1** (0.97, 1.05)	**1** (0.96, 1.06)	**1** (0.95, 1.1)	**1** (0.96, 1.03)	**1** (0.96, 1.08)	**1** (0.95, 1.15)	**1** (0.96, 1.06)	**1** (0.96, 1.08)	**1** (0.94, 1.15)
	Likelihood	44	35	36	40	32	36	44	38	36	38
	Mitigation		**0.19** (1.23, 0)	**0.07** (0.48, 0.07)	**-0.07** (-3.41, 0.09)	**-0.2** (-1.68, -0.01)	**-0.02** (-0.2, 0.65)	**0.15** (-1.06, 0.79)			
	Likelihood		0	10	84	100	72	20			
Dryness	*Amplification factor*	**1.52** (1, 6.43)	**1.02** (0.9, 1.25)	**1.02** (0.91, 1.16)	**1.01** (0.89, 1.15)	**1.06** (0.97, 1.33)	**1.08** (0.98, 1.34)	**1.3** (1.1, 1.94)	**1.05** (0.96, 1.28)	**1.09** (1, 1.31)	**1.4** (1.17, 2.8)
	Likelihood	96	64	63	57	87	90	99	85	95	100
	Mitigation		**-3.75** (-2.47, -6.95)	**-5.88** (-5.28, -5.88)	**-22.86** (-41.1, -18.51)	**0.81** (0.46, 2.92)	**-1.02** (-2.21, 1.73)	**-6.81** (-26.15, -4.37)			
	Likelihood		98	100	99	3	91	100			

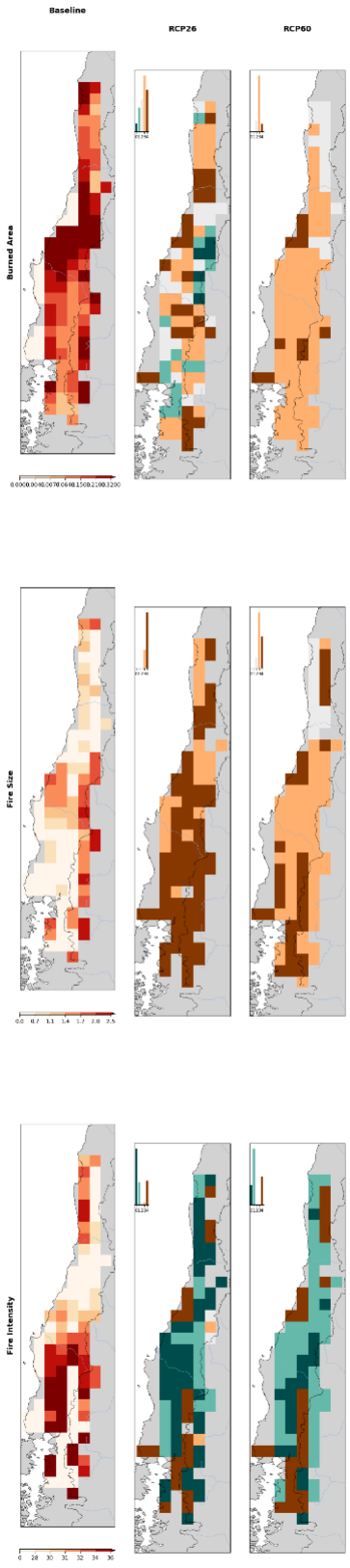


Figure S26. Projected changes in fire characteristics across ISMIP2b GCM future projections taken from Haas et al. (2026). The left column shows modelled baseline conditions for the 2010s, while the right columns show model agreement on the direction of change by 2100 under RCP2.6 (middle) and RCP6.0 (right). Colours indicate the number of models projecting an increase or decrease at each location (brown representing projected increases and blue representing projected decreases). The accompanying histograms summarise the spatial extent of agreement by showing the fraction of the

region where a given number of models agree on the direction of change. Rows correspond (top to bottom) to burned area, fire size, and fire intensity.

Supplementary References

Abatzoglou, J. T., Williams, A. P., and Barbero, R.: Global emergence of anthropogenic climate change in fire weather indices, Geophys. Res. Lett., 46, 326–336, https://doi.org/10.1029/2018gl080959, 2019.

Boussetta, S., Balsamo, G., Arduini, G., Dutra, E., McNorton, J., Choulga, M., Agustí-Panareda, A., Beljaars, A., Wedi, N., Munõz-Sabater, J., de Rosnay, P., Sandu, I., Hadade, I., Carver, G., Mazzetti, C., Prudhomme, C., Yamazaki, D., and Zsoter, E.: ECLand: The ECMWF Land Surface Modelling System, *Atmosphere*, 12, 723, https://doi.org/10.3390/atmos12060723, 2021.

Block, S., Emerson, J. W., Esty, D. C., de Sherbinin, A., Wendling, Z. A., et al. (2024): *2024 Environmental Performance Index*. New Haven, CT: Yale Center for Environmental Law & Policy. Available at: https://epi.yale.edu (last access: 03-January-2026)

Center for International Earth Science Information Network (CIESIN), Columbia University: Gridded Population of the World, Version 4 (GPWv4): Population Density, Revision 11, NASA Socioeconomic Data and Applications Center (SEDAC), https://doi.org/10.7927/H49C6VHW, 2018.

Ciavarella, A., Christidis, N., Andrews, M., Groenendijk, M., Rostron, J., Elkington, M., Burke, C., Lott, F. C., and Stott, P. A.: Upgrade of the HadGEM3-A based attribution system to high resolution and a new validation framework for probabilistic event attribution, Weather and Climate Extremes, 20, 9–32, https://doi.org/10.1016/j.wace.2018.03.003, 2018.

Copernicus Land Monitoring Service (CLMS): Leaf Area Index (LAI) 2014–present (raster 300 m), global, 10-daily, version 1, European Union's Copernicus Land Monitoring Service information, https://doi.org/10.2909/219fdc9f-616b-444b-a495-198f527b4722, last access: 3 March 2026.

Di Giuseppe, F., Pappenberger, F., Wetterhall, F., Krzeminski, B., Camia, A., Libertá, G., and San Miguel, J.: The potential predictability of fire danger provided by numerical weather 94 prediction, J. Appl. Meteorol. Climatol., 55, 2469–2491, https://doi.org/10.1175/jamc-d-15-0297.1, 2016.

Giglio et al., 2025 https://www.sciencedirect.com/science/article/pii/S0034425725004109

Haas, O., Prentice, I.C. and Harrison, S.P., 2026. Wildfires on a changing planet. Nature Communications, 17(1), p.1599.

Hersbach H, Bell B, Berrisford P, et al. The ERA5 global reanalysis. *Q J R Meteorol Soc*. 2020; 146: 1999–2049. https://doi.org/10.1002/qj.3803

Jolly, W. M., Cochrane, M. A., Freeborn, P. H., Holden, Z. A., Brown, T. J., Williamson, G. J., and Bowman, D. M. J. S.: Climate-induced variations in global wildfire danger from 1979 to 2013, Nat. Commun., 6, 7537, https://doi.org/10.1038/ncomms8537, 2015.

Jones, M. W., Abatzoglou, J. T., Veraverbeke, S., Andela, N., Lasslop, G., Forkel, M., Smith, A. J. P., Burton, C., Betts, R. A., van der Werf, G. R., Sitch, S., Canadell, J. G., Santín, C., Kolden, C., Doerr, S. H., and Le Quéré, C.: Global and regional trends and drivers of fire under climate change, Rev. Geophys., 60, https://doi.org/10.1029/2020rg000726, 2022.

Jones, M. W., Andela, N., Brambleby, E., Chuvieco, E., Giglio, L., Kaiser, J. W., Parrington, M., Qu, Y., Torres-Vázquez, M. Á., van der Werf, G. R., and Veraverbeke, S.: State of Wildfires 2025-26: Regional Summaries of Burned Area, Fire Emissions, and Individual Fire Characteristics for National, Administrative and Biogeographical Regions, Zenodo [data set]. https://doi.org/10.5281/zenodo.21262381, 2026.)

Kaplan, J.O., Bigelow, N.H., Prentice, I.C., Harrison, S.P., Bartlein, P.J., Christensen, T.R., Cramer, W., Matveyeva, N.V., McGuire, A.D., Murray, D.F. and Razzhivin, V.Y., 2003. Climate change and Arctic ecosystems: 2. Modeling, paleodata-model comparisons, and future projections. Journal of Geophysical Research: Atmospheres, 108(D19). doi:10.1029/2002JD002559

Kelley, D. I., Burton, C., Di Giuseppe, F., Jones, M. W., Barbosa, M. L. F., Brambleby, E., McNorton, J. R., Liu, Z., Bradley, A. S. I., Blackford, K., Burke, E., Ciavarella, A., Di Tomaso, E., Eden, J., Ferreira, I. J. M., Fiedler, L., Hartley, A. J., Keeping, T. R., Lampe, S., Lombardi, A., Mataveli, G., Qu, Y., Silva, P. S., Spuler, F. R., Steinmann, C. B., Torres-Vázquez, M. Á., Veiga, R., van Wees, D., Wessel, J. B., Wright, E., Bilbao, B., Bourbonnais, M., Gao, C., Di Bella, C. M., Dintwe, K., Donovan, V. M., Harris, S., Kukavskaya, E. A., N'Dri, A. B., Santín, C., Selaya, G., Sjöström, J., Abatzoglou, J. T., Andela, N., Carmenta, R., Chuvieco, E., Giglio, L., Hamilton, D. S., Hantson, S., Meier, S., Parrington, M., Sadegh, M., San-Miguel-Ayanz, J., Sedano, F., Turco, M., van der Werf, G. R., Veraverbeke, S., Anderson, L. O., Clarke, H., Fernandes, P. M., and Kolden, C. A.: State of Wildfires 2024–2025, Earth Syst. Sci. Data, 17, 5377–5488, https://doi.org/10.5194/essd-17-5377-2025, 2025.

Klein Goldewijk, K., Beusen, A., van Drecht, G. and de Vos, M. (2011), The HYDE 3.1 spatially explicit database of human-induced global land-use change over the past 12,000 years. Global Ecology and Biogeography, 20: 73-86. https://doi.org/10.1111/j.1466-8238.2010.00587.x

Kummu, M., Kosonen, M., and Sayyar, M. M.: Downscaled gridded global dataset for gross domestic product (GDP) per capita PPP over 1990–2022, *Sci. Data*, 12, 178, https://doi.org/10.1038/s41597-025-04487-x, 2025.

Li, X., Zhou, Y., Zhao, M. & Zhao, X. A harmonized global nighttime light dataset 1992–2018. *Sci. Data* **7**, 168 (2020) https://doi.org/10.1038/s41597-020-0510-y.

Liu, K., Wang, R., Schrijver, I., and Hoekstra, R.: Can we project well-being? Towards integral well-being projections in climate models and beyond, *Humanit. Soc. Sci. Commun.*, 11, 457, https://doi.org/10.1057/s41599-024-02941-6, 2024.

Lizundia-Loiola, J., Franquesa, M., Khairoun, A., Chuvieco, E. Global burned area mapping from Sentinel-3 Synergy and VIIRS active fires, Remote Sensing of Environment, Volume 282, 2022, 113298, ISSN 0034-4257, https://doi.org/10.1016/j.rse.2022.113298

Lizundia-Loiola et al., 2020 https://www.sciencedirect.com/science/article/pii/S0034425722004047

Lopez, P. A Lightning Parameterization for the ECMWF Integrated Forecasting System. *Mon. Weather Rev.* **144**, 3057–3075 (2016).

McNorton, J. R. and Di Giuseppe, F.: A global fuel characteristic model and dataset for wildfire prediction, *Biogeosciences*, 21, 279–300, https://doi.org/10.5194/bg-21-279-2024, 2024.

Meijer, J. R., Huijbregts, M. A. J., Schotten, K. C. G. J., and Schipper, A. M.: Global patterns of current and future road infrastructure, *Environ. Res. Lett.*, 13, 064006, https://doi.org/10.1088/1748-9326/aabd42, 2018.

Meiyappan, P., Jain, A.K. Three distinct global estimates of historical land-cover change and land-use conversions for over 200 years. *Front. Earth Sci.* **6**, 122–139 (2012). https://doi.org/10.1007/s11707-012-0314-2

Muñoz-Sabater, J., Dutra, E., Agustí-Panareda, A., Albergel, C., Arduini, G., Balsamo, G., Boussetta, S., Choulga, M., Harrigan, S., Hersbach, H., Martens, B., Miralles, D. G., Piles, M., Rodríguez-Fernández, N. J., Zsoter, E., Buontempo, C., and Thépaut, J.-N.: ERA5-Land: a state-of-the-art global reanalysis dataset for land applications, Earth Syst. Sci. Data, 13, 4349–4383, https://doi.org/10.5194/essd-13-4349-2021, 2021.

Pesaresi, M. & Politis, P. GHS-BUILT-S R2023A – GHS built-up surface grid, derived from Sentinel-2 composite and Landsat, multitemporal (1975–2030). Accessed 12 March 2025. https://doi.org/10.2905/9F06F36F-4B11-47EC-ABB0-4F8B7B1D72EA.

Qu, Y., Jones, M. W., Brambleby, E., Hunt, H. G. P., Pérez-Invernón, F. J., Yebra, M., Zhao, L., Moris, J. V., Janssen, T., and Veraverbeke, S.: A new global gridded lightning dataset with high spatial and temporal resolution, EGU General Assembly 2025, Vienna, Austria, 27 Apr–2 May 2025, EGU25-8351, https://doi.org/10.5194/egusphere-egu25-8351, 2025.

Soci, C., Hersbach, H., Simmons, A., Poli, P., Bell, B., Berrisford, P., et al. (2024) The ERA5 global reanalysis from 1940 to 2022. Quarterly Journal of the Royal Meteorological Society, 150(764), 4014–4048. Available from: https://doi.org/10.1002/qj.4803

Stocker, B. D., Wang, H., Smith, N. G., Harrison, S. P., Keenan, T. F., Sandoval, D., Davis, T., and Prentice, I. C.: P-model v1.0: an optimality-based light use efficiency model for simulating ecosystem gross primary production, Geosci. Model Dev., 13, 1545–1581, https://doi.org/10.5194/gmd-13-1545-2020, 2020.

Torres-Vazquez et al., 2026: Torres-Vázquez, M. Á., Segura-Garcia, C., Turco, M., Khairoun, A., Pettinari, M. L., Solano-Romero, E., García, M., Oliva, P., Jones, M. W., and Chuvieco, E.: MRBA60: Long-term consistent global burned area dataset from Sentinel-3 and MODIS products, Scientific Data, under revision.

Turco et al. (2026) Turco, M., Jones, M., & Di Giuseppe, F. (2026). State of Wildfires 2025-26: Anomalies in Extreme Fire Weather Days by Continent, Biome, Country, and Administrative Region (2026.0) [Data set]. Zenodo. https://doi.org/10.5281/zenodo.20757872

United Nations. *Human Development Report 2025*. Human Development Reports (2025). Accessed 30 October 2024. https://hdr.undp.org/content/human-development-report-2025.

Vitolo, C., Di Giuseppe, F., Barnard, C., Coughlan, R., San-Miguel-Ayanz, J., Libertá, G., and Krzeminski, B.: ERA5-based global meteorological wildfire danger maps, Sci. Data, 7, 216, https://doi.org/10.1038/s41597-020-0554-z, 2020.

van Wagner, C. E.: Development and structure of the Canadian forest fire weather index system, cabidigitallibrary.org, https://doi.org/10.5555/19910646918, 1987.

World Bank (2025): Worldwide Governance Indicators, 2025 Update, available at: https://www.worldbank.org/en/publication/worldwide-governance-indicators (last access: 04 January 2026).